

Internal tides off the Amazon shelf Part I: importance for the structuring of ocean temperature during two contrasted seasons

Fernand [Assene¹Assene¹](#), Ariane Koch-[Larrouy²Larrouy²](#), Isabelle [Dadou³Dadou³](#), Michel [Tchilibou⁴Tchilibou⁴](#), Guillaume [Morvan⁵Morvan⁵](#), Jérôme [Chanut⁶Chanut⁶](#), Alex Costa da [Silva⁷Silva⁷](#), Vincent [Vantrepotte⁸Vantrepotte⁸](#), Damien [Allain⁹Allain⁹](#), Trung-Kien [Tran¹⁰Tran¹⁰](#)

^{1, 2, 3, 5, 9}[Université⁹Université](#) de Toulouse, LEGOS ([CNES/CNRS/IRD/UPS/CNESUT3](#)), Toulouse, France

^{1, 6}[Mercator⁶Mercator](#) Ocean International, 31400, Toulouse, France

⁴[Collecte⁴Collecte](#) Localisation Satellites (CLS), 31500, Ramonville Saint-Agne, France

⁷[Departamento⁷Departamento](#) de Oceanografia da Universidade Federal de Pernambuco, DOCEAN/UFPE, Recife, Brazil

^{8, 10}[Laboratoire¹⁰Laboratoire](#) d'Océanologie et de Géosciences (LOG), 62930, Wiméreau, France

Correspondence to: Fernand Assene (fassene@mercator-ocean.fr)

Abstract

The impact of ~~the tides~~ (internal and [external](#)) [barotropic tides](#) on the vertical and horizontal ~~structure of~~ temperature [structure](#) off the Amazon River ~~is~~[was](#) investigated during two highly contrasted seasons (AMJ: April-May-June and ASO: August-September-October) over a three-year period from 2013 to 2015. Twin regional simulations, with and without tides ~~are, were~~ used to highlight the general effect of tides. The [findings reveal that](#) tides ~~tend to cool down~~[have a cooling effect on](#) the ocean from the surface (~ 0.3 °C) to above the thermocline (~ 1.2 °C), ~~and to warm while warming~~ it up below the thermocline (~ 1.2 °C). The heat budget analysis ~~leads to~~[indicates that](#) the ~~conclusion that~~ vertical mixing [represents](#) the dominant process ~~that drives these~~[driving](#) temperature variations within the mixed layer, while it is associated with both horizontal and vertical advection ~~below~~ to explain temperature variations ~~below~~. The ~~intensified~~[increased](#) mixing in the ~~simulations~~[simulations](#) including tides is attributed to ~~the~~ breaking of internal tides (IT) on their generation sites over the shelf break and offshore along their propagation pathways. ~~While over~~[Over](#) the shelf, ~~the~~ mixing is driven by the dissipation of the ~~external~~[barotropic](#) tides. In addition, ~~the~~ vertical terms of the heat budget equation ~~show exhibit~~ wavelength patterns typical of mode-1 IT. [The study highlights the key role of tides and particularly how IT-related vertical mixing shapes the ocean temperature off the Amazon. Furthermore, we found that tides impact the interactions between the upper ocean interface and the overlying atmosphere. They contribute significantly to increasing the net heat flux between the atmosphere and the ocean, with a notable seasonal variation from 33.2% in](#)

37 AMJ to 7.4% in ASO seasons. This emphasizes the critical role of tidal dynamics in
38 understanding regional-scale climate.

39 ~~Moreover, we found that the tides can impact the interactions between the upper ocean~~
40 ~~interface and the overlying atmosphere. They account for a significant proportion of the net~~
41 ~~heat flux between the atmosphere and the ocean, with a marked seasonal variation of 33.2% in~~
42 ~~AMJ to 7.4% in ASO seasons. Tidal dynamics is therefore critical to understand the climate at~~
43 ~~regional scale. This study highlights the key role of tides and particularly how IT-related vertical~~
44 ~~mixing helps to shape ocean temperature off the Amazon.~~

45 **Keywords:** Amazon shelf break, modeling, internal tides, mixing, temperature cooling, heat
46 flux, ~~modeling, satellite data.~~

47 **I. Introduction**

48 ~~Temperature and its spatial structure play a crucial role in ocean, including~~In the ocean,
49 many processes depend on temperature. These processes include water mass formation (Swift
50 and Aagaard, 1981; Lascaratos, 1993; Speer et al., 1995), the transport and mixing of ~~other~~
51 ~~tracers in the ocean and,~~ exchanges with other biosphere compartments (Archer et al., 2004,
52 Rosenthal et al., 1997), and, ~~most importantly on,~~ surface heat exchange at the interface with
53 the atmosphere (Clayson and Bogdanoff, 2013; Mei et al., 2015) ~~and can thus), which~~ which
54 significantly influence the climate (Li et al., 2006; Collins et al., 2010). ~~This~~The oceanic thermal
55 structure can be modified at various spatial and temporal scales, through ~~different~~external
56 processes ~~external to the ocean like~~such as solar radiation, heat exchanges with the atmosphere,
57 winds, precipitation, and freshwater inputs from rivers, ~~and by its~~as well as internal processes
58 ~~such as including~~ mass transport by currents and eddies (e.g., Aguedjou et al., 2021), mixing by
59 turbulent diffusion (Kunze et al., 2012), and the dissipation of internal waves (Barton et al.,
60 2001; Smith et al., 2004; Salamena et al., 2021). ~~Finally~~Additionally, bottom friction of ~~the~~
61 barotropic tidal currents ~~may also produce~~can lead to intensified mixing ~~especially for,~~
62 particularly in shallow water conditions (~~e.g., over a shelf, (see Lambeck and Runcorn, 1977;~~
63 Le Provost and Lyard, 1997)), and significantly modify ocean temperature in surface layers (Li
64 et al., 2020).

65 The barotropic tides, also called external tides, ~~are~~serve as the ~~main~~primary source for
66 generating internal waves ~~generation. The external. When barotropic~~ tides, ~~when interacting~~
67 interact with sharp topography (~~e.g., such as~~ ridge, sea mounts, shelf break) in a stratified ocean,
68 they generate internal tides, (IT) that propagate and dissipate in the ocean interior causing

69 diapycnal mixing (Baines, 1982; Munk and Wunsch, 1998; Egbert and Ray, 2000). ~~A number~~
70 ~~of~~ ~~Several~~ observational and modelling studies have ~~shown~~ ~~demonstrated~~ that this dissipation
71 occurs at the generation sites, ~~at the~~ ~~through~~ reflection ~~at~~ the ~~ocean~~ bottom, or ~~close to~~ ~~near~~ the
72 surface when the energy rays interact with the ~~thermocline and~~ pycnocline (among others:
73 Laurent and Garrett, 2002; Sharples et al., 2007, 2009; Koch-Larrouy et al., 2015; Nugroho et
74 al., 2018; Whalen et al., 2012). IT also dissipate or lose energy ~~by~~ ~~through~~ wave-wave
75 interactions or when they interact with mesoscale or fine-scale structures (Vlasenko and
76 Stashchuk, 2006; Dunphy and Lamb, 2014).

77 The role of ~~internal tides on~~ ~~IT in shaping~~ the ocean's thermal structure has ~~been the~~
78 ~~subject of growing~~ ~~garnered increasing~~ interest and ~~has been the focus of~~ numerous studies in
79 recent years. In the ~~Hawaii~~ shallow shelf surface waters ~~of Hawaii~~, Smith et al. (2016)
80 ~~report~~ ~~reported~~ that IT can induce surface cooling ~~ranging~~ from 1 °C to -5 °C. ~~For~~ ~~Similarly, in~~
81 the Indonesian region, ~~IT induce an annual mean surface cooling of 0.5 °C (studies by~~ Koch-
82 Larrouy et al., (2007, 2008;), Nagai and Hibiya, (2015) and Nugroho et al., (2018) ~~found~~
83 that ~~decreases~~ ~~IT lead to an average surface cooling of 0.5 °C, which subsequently reduces~~ local
84 atmospheric convection, ~~which and results in~~ ~~turn reduces a 20% decrease in~~ precipitation ~~by~~
85 ~~20%. They can therefore fulfil a relevant.~~ ~~Therefore, IT play a significant role on~~ ~~in the~~ regional
86 climate ~~dynamics~~ (Koch-Larrouy et al., 2010; Sprintall et al., 2014, 2019). Furthermore, ~~in the~~
87 ~~Andaman Sea~~, Jithin and Francis (2020) ~~showed~~ ~~demonstrated~~ that ~~internal tides in the Andaman~~
88 ~~Sea, IT can affect~~ ~~influence~~ the temperature ~~in~~ ~~of~~ deep waters (> 1600 m), ~~leading to~~ ~~resulting in~~
89 a warming ~~effect~~ of about 1–2 °C. ~~But~~ ~~However, the impact of IT on temperature~~ off the Amazon
90 plateau, ~~their impact on the thermal structure of the ocean~~ is still ~~poorly~~ ~~not well~~ understood.

91 Our study focuses on the oceanic region of northern Brazil off the Amazon River. This
92 region ~~exhibits a variation~~ ~~experiences variations~~ in the wind ~~position~~ ~~patterns~~ and hence the
93 position of the Intertropical Convergence Zone (ITCZ) ~~during~~ ~~throughout~~ the year. ~~This~~ ~~These~~
94 ~~variations~~ directly ~~influence~~ ~~impact~~ the discharge of the Amazon River, oceanic circulation,
95 eddy kinetic energy (EKE) and ~~the~~ stratification (Muller-Karger et al., 1988; Johns et al., 1990;
96 Xie and Carton, 2004). ~~Hence~~ ~~Consequently~~, two ~~very~~ ~~contrasting~~ ~~contrasted~~ seasons
97 ~~form, emerge~~: April-May-June (AMJ) and August-September-October (ASO). ~~The~~ AMJ (vs.
98 ASO) ~~is characterized by~~ ~~season features~~ an increasing (vs. decreasing) river discharge, ~~there is~~
99 ~~a~~ stronger (vs. ~~smaller~~ ~~weaker~~) and shallower (vs. deeper) pycnocline. ~~The, while the~~ North
100 Brazilian Current (NBC) and ~~eddy kinetic energy (EKE)~~ are weaker (vs. stronger) (Aguedjou
101 et al., 2019, Tchilibou et al., 2022). ~~For~~ ~~During~~ AMJ season, NBC forms a weak equatorial

102 ~~retroreflection that contributes to the Equatorial Under-Current. In~~ the ASO season, ~~the~~when
103 ~~NBC strengthens, it forms a~~ stronger NBC ~~develops a~~ retroreflection (NBCR) between 5°–8° N
104 ~~that in the northwest, which~~ feeds the North Equatorial Counter-Current (NECC) ~~transporting~~
105 ~~the and transports~~ water masses ~~towards the east of~~ eastwards into the tropical Atlantic. ~~The~~This
106 ~~intensified~~ retroreflection ~~also generates very~~ gives rise to large anticyclonic eddies (~~called~~ NBC
107 Rings) ~~exceeding, which can exceed~~ 450 km in diameter (Didden and Schott, 1993; Richardson
108 et al., 1994; Garzoli et al., 2003), ~~which in turn transport~~). ~~These eddies play a role in~~
109 ~~transporting~~ water masses towards the Northern Hemisphere (Bourles et al., 1999; Johns et al.,
110 1998; Schott et al., 2003).

111 ~~Internal tides~~In this region, IT are generated ~~on~~at the sharp shelf break ~~featured by a,~~
112 ~~where the~~ depth ~~decreasing~~decreases from 200–2000 m over ~~some~~few tens of kilometers
113 (Fig.1). Six main sites (A to F) have been identified, with the most intense ~~sites~~, A and B,
114 located in the southern part of the region (Fig.1; Magalhaes et al., 2016, Tchilibou et al., 2022).
115 Previous studies have ~~shown~~indicated that ~~the propagation of IT~~ in this region ~~IT propagation~~
116 is modulated by ~~the~~seasonal variation ~~of the~~in currents (Magalhaes et al., 2016; Lentini et al.,
117 2016; Tchilibou et al., 2022). ~~In addition, seasonal variations in~~ Moreover, changes in
118 stratification ~~induce changes in~~ throughout different seasons affect the ~~activity of~~ internal tide's
119 ~~activity, with in tides. In~~ AMJ (vs. ASO) ~~season, there is~~ a stronger (vs. smaller) energy
120 conversion and a stronger (vs. smaller) local dissipation of IT energy (Barbot et al., 2021,
121 Tchilibou et al., 2022). The interaction between the weaker (vs. stronger) background
122 circulation and IT ~~leads to less~~results in fewer (vs. more) incoherent or non-stationary internal
123 tides (Tchilibou et al., 2022).

124 During the ASO season, cold water (~~with~~ temperature below 27.6 °C), associated with
125 the western extension of the Atlantic Cold-water Tongue (ACT) ~~runs~~, ~~flows into~~ the region
126 from the south and ~~runs~~ along the edge of the continental shelf up to ~~about~~ 3°N,
127 ~~establishing~~forming a cold cell ~~often referred to~~known as seasonal upwelling (Lentz and
128 Limeburner, 1995; Neto and da Silva, 2014). ~~Modelling studies, with and without tides, have~~
129 ~~shown~~Based on *in situ* observations, the latter suggest that this ~~upwelling~~cooling is
130 ~~affected~~backed by the tides. ~~Cooling is more realistic when tides are included (vertical~~
131 ~~advection triggered by the NBC. Alternatively,~~ Ruault et al., (2020). ~~However, these analyses~~
132 ~~cannot determine what processes are at work. For example, it is not yet explicit whether the~~
133 ~~tidal induced cooling is due to mixing on the shelf produced by barotropic tides, or to the mixing~~
134 ~~produced by baroclinic tides at their generation sites and propagation pathways. Based on in~~

~~situ observations, Neto and da Silva (2014) suggest instead that it is the vertical advection triggered by the NBC that can explain the cooling observed at the surface.) conducted a modeling study, comparing simulations with and without tides, and demonstrated that the inclusion of tides resulted in a more realistic cooling effect on this upwelling. However, it remains unclear whether the cooling is a result of mixing on the shelf caused by barotropic tides or mixing caused by baroclinic tides at their generation sites and propagation pathways.~~

To answer the previous questions, we use a high-resolution model (1/36°) with and without explicit tidal forcing and a satellite SST product, ~~with the.~~ Our aim of highlighting is to examine the impact of tides on the temperature structure and quantify the associated processes. ~~We distinguish the analysis_~~ for the two contrasted seasons (AMJ and ASO) described above. ~~The Section II provides a description of the~~ SST product, our model, and the methods used ~~are described in section II.~~ The validation of ~~certain tidal~~ characteristics ~~of the barotropic and baroclinic tides and of,~~ as well as the temperature is presented in section III. ~~The Section IV focuses on the analysis of the~~ impacts of ~~IT~~tides on the temperature structure, ~~and the associated processes, as well as~~ the influence of tides on heat exchange at the atmosphere-ocean interface, ~~and the processes involved, are analyzed in section IV.~~ The discussion and ~~the~~ summary of the obtained results are presented in ~~section~~sections V and VI, respectively.

II. Data and Methods

II.1. Satellite Data: TMI SST

This dataset is derived from Tropical Rainfall Measurement Mission (TRMM), which performs measurements using onboard TRMM Microwave Imager (TMI). The microwaves can penetrate clouds and are therefore crucially important for data acquisition in low latitude regions, cloudy covered during long periods of raining seasons. We use TMI data products v7.1, which represents is the most recent version of TMI SST. It contains a daily mean of SST with a 0.25°×0.25° grid resolution (~25 km). This SST is obtained by through inter-calibration of TMI data with other microwave radiometers. The TMI SST full description and inter-calibration algorithm are detailed in Wentz (2015).

II.2. The NEMO Model: *AMAZON36* configuration

The numerical model used in this study is the Nucleus for European Modelling of the Ocean (~~NEMO v4~~NEMO v4.0.2, Madec et al., 2019). The specific configuration designed for ~~our purpose~~this study is called *AMAZON36* and covers the western tropical Atlantic region from the Amazon River mouth to the open ocean. Other configurations exist in this region, ~~but~~ either

167 ~~they~~ have a coarse grid (~~1/4°~~1/4°, Hernandez et al., 2016), or, when the grid is fine (1/36°)
168 ~~they~~1/36°, do not extend ~~very~~-far enough eastwards and ~~therefore~~ exclude most of the site B
169 (Ruault et al., 2020). The current AMAZON36 configuration ~~avoids~~overcomes these ~~two~~
170 limitations. The grid resolution is ~~1/36°~~1/36°, and the domain ~~lies~~spans between 54.7°W–
171 35.3°W and 5.5°S–10°N (Fig.1). In this way, we capture the internal tides radiating from all the
172 generating sites on the Brazilian shelf break. The vertical grid ~~comprises~~consists of 75 vertically
173 fixed z-coordinates levels, with a narrower grid refinement near the surface ~~with,~~ comprising
174 23 levels in the first 100 m. ~~Cell,~~ whereas cell thickness reaches 160 m ~~when approaching~~near
175 the bottom. The horizontal and vertical resolutions of the grid are therefore fine enough to
176 resolve low-mode ~~internal tides.~~IT. This grid resolution has ~~already~~-been previously used for
177 ~~this~~similar purpose in this region (e.g., Tchilibou et al., 2022).

178 A third order upstream biased scheme (UP3) with built-in diffusion is used for
179 momentum advection, while tracer advection relies on a 2nd order Flux Corrected Transport
180 (FCT) scheme (Zalesak, 1979). A Laplacian isopycnal diffusion with a constant coefficient of
181 ~~20 m².s⁻¹~~20 m².s⁻¹ is used for tracers. The temporal integration is achieved thanks to a
182 leapfrog scheme combined with an Asselin filter to damp numerical modes, with a baroclinic
183 time step of 150 s. The ~~k=εk-ε~~ turbulent closure scheme is used for vertical diffusion. Bottom
184 friction is quadratic with a bottom drag coefficient of ~~2.5×10⁻³~~2.5×10⁻³, while lateral wall
185 free-slip boundary conditions are prescribed. A time splitting technique is used to resolve the
186 free surface, with the barotropic part of the dynamical equations integrated explicitly.

187 We use the ~~2020's~~2020 release of the General Bathymetric Chart of the Oceans, which
188 has been interpolated onto the ~~model~~model's horizontal grid, with the minimal depth set to 12.8
189 m. The model is forced at the surface by the ERA-5 atmospheric reanalysis (Hersbach et al.,
190 2020). ~~The river discharges~~River runoff are based on monthly means from hydrology
191 simulation of the Interaction Sol-Biosphère-Atmosphère model (~~see details in~~ISBA,
192 <https://www.umr-cnrm.fr/spip.php?article146&lang=en>) and are prescribed as surface mass
193 sources with null salinity, ~~and we.~~ We use a ~~multiplicative factor of~~90% of ISBA runoff based
194 on a comparison with the HYBAM interannual runoff timeseries (~~see details in~~([http://www.ore-](http://www.ore-hybam.org)
195 [hybam.org](http://www.ore-hybam.org))). The model is forced at its open boundaries by the fifteen major tidal constituents
196 (M₂, S₂, N₂, K₂, 2N₂, MU₂, NU₂, L₂, T₂, K₁, O₁, Q₁, P₁, S₁, and M₄) and barotropic currents,
197 derived from FES2014 atlas (Lyard et al., 2021). In addition, we prescribe to the open
198 boundaries, ~~we prescribe~~ the temperature, salinity, sea level, current velocity and derived
199 baroclinic velocity from the recent MERCATOR-GLORYS12 v1 assimilation data (Lellouche

et al., 2018) ~~for temperature, salinity, sea level, current velocity and derived baroclinic velocity.~~

The ~~simulation was~~ simulations were initialized on ~~the 1st of~~ January 1, 2005, and ran for 11 years until December 2015. ~~It was found that the model achieved a seasonal cycle equilibrium after two years. However, for~~ this study, ~~we use our focus lies on a~~ three-year ~~model outputs period~~ from January 2013 to December 2015. ~~Indeed, the model has reached an equilibrium in terms of seasonal cycle after 2 years. A twin model configuration without tides is used to~~ To highlight the influence of tides on the temperature structure-, we use a twin model configuration without tidal forcing.

II.3. Methods

II.3.1. Tide energy budget

We follow Kelly et al. (2010) to separate barotropic and baroclinic tide constituents. There is no separation following vertical modes, then we analyze the total energy for all the resolved propagation modes for a given tidal frequency. Note that the barotropic/baroclinic tide separation is performed directly by the model for better accuracy. We have only analyzed the M_2 harmonic which is the major tidal constituent in this region (Prestes et al., 2018; Fassoni-Andrade et al., 2023), representing $\sim 70\%$ of the tidal energy (Beardsley et al., 1995; Gabioux et al., 2005).

The energy budget equations of barotropic and baroclinic ~~tide energy budget equations~~ tides are obtained assuming that the energy tendency, the nonlinear advection and the forcing terms are small (Wang et al., 2016). ~~Then, the~~ The remaining equations are reduced to the balance between the energy dissipation, the divergence of the energy flux, and the energy conversion from barotropic to baroclinic (e.g., Buijsman et al., 2017; Tchilibou et al., 2018, 2020; Jithin and Francis, 2020; Peng et al., 2021) :

$$D_{bt} + \nabla_h \cdot F_{bt} + C \approx 0 \quad (1)$$

$$D_{bc} + \nabla_h \cdot F_{bc} - C \approx 0 \quad (2)$$

bt and bc indicate the barotropic and baroclinic terms, respectively, D is the depth-integrated energy dissipation, which can be understood as a proxy of the real dissipation since D may encompass the energy loss of non-linear terms and/or numerical dissipation (see Nugroho et al., 2018), $\nabla_h \cdot F$ represents the divergence of the depth-integrated energy flux, whilstwhile C is

230 the depth-integrated barotropic-to-baroclinic energy conversion, i.e., the amount of incoming
 231 barotropic energy converted into internal tides energy over the steep topography, with:

$$232 \quad C = \langle \nabla H \cdot U_{bt} P_{bc}^* \rangle \quad (3)$$

$$233 \quad F_{bt} = \langle U_{bt} P_{bt} \rangle \quad (4)$$

$$234 \quad F_{bc} = \int_H^\eta \langle U_{bc} P_{bc} \rangle dz \quad (5)$$

235 where the angle bracket $\langle \cdot \rangle$ denotes the average over a tidal period, ∇H is the slope of the
 236 bathymetry, U is the current velocity, P_{bc}^* is the baroclinic pressure perturbation at the bottom,
 237 H is the bottom depth, η the surface elevation, P is the pressure, then F is the energy flux and
 238 emphasizes/indicates the path of ~~the~~ tides.

239 II.3.2. 3-D heat budget equation for temperature

240 The three-dimensional temperature budget was computed online and further analyzed.
 241 It is the balance between the total temperature trend and the sum of the temperature advection,
 242 diffusion and solar radiative and non-solar radiative fluxes (e.g., Jouanno et al., 2011;
 243 Hernandez et al., 2017). The three-dimensional heat budget equation for temperature is
 244 expressed as follows:

$$245 \quad \partial_t T = \underbrace{-u\partial_x T - v\partial_y T - w\partial_z T}_{ADV} + LDF - \underbrace{\partial_z(K_z \partial_z T)}_{ZDF} - \underbrace{\partial_z(K_z \partial_z T)}_{ZDF} + Forcing + Asselin$$

246 (6)

247 Herehere T is the model potential temperature, (u, v, w) are the velocity components in the $(x,$
 248 $y, z)$ [respectively eastward, northward and upward] directions, ADV is the 3-D tendency term
 249 from the advection routine of the NEMO code (~~from the~~ left to right: zonal, meridional and
 250 vertical terms). Note that in our model, ADV includes nonlinear effect between the temperature
 251 and the currents and leads to some diffusivity of the temperature due to numerical dissipation
 252 of the FCT advection scheme (Zalesak, 1979) in contrast to some non-diffusive advection
 253 scheme like in Leclair and Madec (2009). In previous studies, for lower resolution ($1/4^\circ$), this
 254 mixing has been quantified to be responsible for 30% of the dissipation as part of the high-
 255 frequency workeffect of the diffusion (Koch-Larrouy et al., 2008). We expect here at $1/36^\circ$
 256 resolution that this effect will be smaller but still non negligible. This will be discussed in the
 257 last section. Note that explicit separation of this effect is beyond the scope of our study.
 258 Furthermore, tides are primarily linear in surface water, however, non-linear effects intensify
 259 due to bottom friction for barotropic tides or as a result of IT breaking. Consequently, we

260 ~~anticipate a corresponding increase in ADV . ZDF represents~~denotes the vertical diffusion, LDF
261 is the lateral diffusion, $Forcing$ is the sum of tendency of temperature due to penetrative solar
262 radiation, which includes a vertical decaying structure, and the non-solar heat flux (sum of the
263 latent, sensible, and net infrared fluxes) at the surface layer, and $Asselin$ corresponds to the
264 numerical diffusion for the temperature.

265 III. Model validation

266 In this ~~subsection~~section, we assess the quality of our simulations by verifying whether
267 they are in good agreement with the observations and other reference data. Firstly, for the
268 barotropic and baroclinic characteristics of the M_2 tides for the year 2015, and finally for the
269 temperature from 2013 to 2015.

270 III.1. M_2 Tides in the model

271 We initially examined the barotropic SSH and there is a good agreement in both
272 amplitude (~~color shading~~) and phase (~~solid contours~~) between FES2014 and the model, Fig.2a
273 and Fig.2b, respectively. ~~Nevertheless~~However, near the coast, ~~some few~~ differences in
274 ~~amplitude~~ are observed ~~in amplitude~~. The ~~model's~~ SSH amplitude ~~of the model~~ is lower ($\sim +50$
275 cm) north of the mouth of the Amazon. ~~However, shoreward and on the southern part of the~~
276 ~~mouth, the model, while it~~ overestimates the amplitude by $\sim +20$ cm and $\sim +40$ cm,
277 respectively, ~~shoreward and on the southern part of the mouth~~. These biases are of ~~the same~~
278 ~~order of a similar~~ magnitude as ~~those reported in~~ Ruault et al. (2020). The flux of the barotropic
279 tidal energy flowing inshore is ~~represented by the black arrows depicted~~ in Fig.2c and Fig.2d
280 for FES2014 and the model, respectively. A ~~fraction~~portion of this energy is converted into
281 baroclinic tidal energy over the steep slope of the bathymetry. We compared the depth-
282 integrated barotropic-to-baroclinic energy conversion rate (C) between FES2014 and the
283 model, ~~color shading in~~ Fig.2c and Fig.2d, respectively. The model ~~does reproduce~~successfully
284 ~~reproduces~~ the same conversion patterns of FES2014 over the slope, but ~~hardly less~~ offshore
285 between 42°W – 35°W and 7°N – 10°N . ~~This leads to an~~As a result, our model overall
286 ~~underestimate of~~underestimates C of about 30% by our model ~~approximately 30%~~. Niwa and
287 Hibiya (2011) ~~have shown~~demonstrated that C increases with ~~higher~~ bathymetry resolution,
288 ~~meaning indicating~~ that there is more conversion with the FES2014 grid (~ 1.5 km) compared to
289 our grid (~ 3 km). ~~In addition, FES2014 (vs. our model) is a barotropic (vs. baroclinic) model,~~
290 ~~which may be a source of some differences since it solves different set of equations.~~

291 Another partportion of the barotropic energy is dissipated on the shelf bythrough bottom
292 friction ~~and induces, leading to~~ mixing from the bottom (Beardsley et al., 1995; Gabioux et al.,
293 2005; Bessières, 2007; Fontes et al. (2008)). Most of the dissipation of barotropic energy (D_{bt})
294 occurs in the middle and inner shelf between 3°S–4°N (Fig.2e) in good agreement withwith a
295 mean value of about 0.25 W.m⁻² (Fig.2e). The location of this dissipation aligns well with
296 previous studies of Beardsley et al. (1995) and Bessières (2007). The remaining barotropic
297 energy propagates over hundreds of kilometers into the estuarine systems of this region (Kosuth
298 et al., 2009; Fassoni-Andrade et al., 2023).

299 ~~For the internal tides, their~~The energy flux of IT (F_{bc} , black arrows in Fig.2f) shows)
300 indicates that they propagate from the slope towards the open ocean. (Fig.2f). F_{bc}
301 highlightsindicates the existence of six main sites of IT generation on the slope. ~~Two of these~~
302 ~~are more important (, with sites A and B) regarding being particularly significant in terms of~~
303 their higher and far extended energy flux, in good agreement with previous studies (Magalhaes
304 et al. (., 2016); Barbot et al. (., 2021) and Tchilibou et al. (., 2022)). From these two main sites,
305 internal tidesIT spread over nearly 1000 km, and dissipate their energy. Color shading in Figure
306 2f shows theThe model's depth-integrated internal tides energy dissipation (D_{bc}). We found
307 that about) is at least two times weaker than barotropic energy dissipation, with a mean value
308 of 0.1 W.m⁻² (Fig.2f). Approximately 30% of ~~theIT~~ energy is dissipated locally over generation
309 sites (not shown), in good agreementconsistent with the findings of Tchilibou et al. (2022). The
310 remaining partportion is dissipated offshore along the propagation path. This offshore
311 dissipation is more extended along path A, ~300 km from the slope, with two patternsbeams
312 spaced approximately by an average wavelengthdistance of 120–150 km corresponding to
313 mode-1 propagation. Whilewavelength. On the other hand, there is less offshore dissipation
314 along path B, occurring around 100–200 km from the slope (Fig.2f).

315 Another criticalimportant characteristic of IT is their SSH imprints along the
316 propagation pathway. ~~We compared anThe~~ estimate of this signature deduced from the
317 altimeter tracks (Fig.2g) produced by Zaron (2019) is compared with our model (Fig.2h), with
318 the shelf masked over 150 m depth. Our model is inshows good agreement with this product,
319 albeit with ana slight overestimation of ~~the order of~~ about ~1.5 cm on the SSH maxima. It
320 is relevant to noteworth noting that the model's baroclinic SSH ~~of our model~~ is an average over
321 the year 2015, whilstwhile the satellite estimate is an average over a longer period of about 20
322 years. ~~This means that~~ The longer period of the satellite estimate may introduce greater

323 variability ~~of~~ in the altimeter tracks ~~is greater due to the longer period, which may reduce,~~
324 ~~potentially reducing~~ the amplitude of the estimates and ~~explain~~ explaining the ~~small~~ slight
325 differences ~~with the model~~ in the positioning and amplitude of the maxima.

326 III.2. Temperature validation

327 Figure 3 shows the mean SST over the entire 2013–2015 period for TMI SST (Fig.3a),
328 the tidal ~~simulations~~ simulations (Fig.3b) and the non-tidal ~~simulations~~ simulations (Fig.3c),
329 ~~then~~). We obtain the bias between TMI SST and the two simulations ~~is obtained~~ by linear
330 interpolation of the simulations data on the observation grid. The ~~simulations~~ simulations with
331 tides accurately ~~reproduces~~ reproduce the spatial distribution of the observations ~~both for, as~~
332 ~~indicated by the weak bias ($< \pm 0.1^\circ\text{C}$) with TMI SST. This is particularly evident for the~~
333 cooling on the shelf around 47.5°W and to the southeast between 40°W – 35°W and 2°S – 2°N ,
334 ~~as shown by the weak bias, $< \pm 0.1^\circ\text{C}$, with TMI~~ (Fig.3d). ~~This cooling is inaccurately~~
335 ~~reproduced by~~ In contrast, the non-tidal ~~simulation which exhibits~~ simulations exhibit a warm
336 bias of about 0.3°C ~~in this cooling region~~ (Fig.3e). To the northeast, between 50°W – 54°W
337 and 3°N – 8°N in the Amazon plume, the SST of the non-tidal ~~simulations~~ simulations is in better
338 agreement with the observations, while the SST of the tidal ~~simulations~~ simulations is about $>$
339 0.6°C cooler than TMI SST (Fig.3d). ~~The same~~ This bias is ~~obtained~~ consistent with other
340 ~~models that include tides~~ in this northern zone ~~by other models including tides~~ (e.g., Hernandez
341 et al., 2016, 2017; Gévaudan et al. (2022). Far offshore, between 50°W – 40°W and 6°N – 10°N ,
342 both simulations ~~reveal~~ exhibit a negative bias of about 0.2 – 0.3°C (Fig.3d–e). We averaged
343 the observations and ~~the~~ interpolated simulation data ~~in~~ within the dashed box (see Fig.3a–c),
344 with a depth ~~of less than~~ 200 m masked. This location ~~is around of the boxes comprises~~ IT
345 generation sites and ~~on~~ part of their pathways. ~~Then, we compute~~ We then computed the
346 seasonal cycle of the three products (Fig.3f). The tidal and non-tidal simulations ~~of the model~~
347 ~~reproduce~~ accurately reproduce both the seasonal cycle and the standard deviation of the
348 observations, with a low RMSE ~~root mean square errors~~ of ~~$\sim 2 \cdot 10^{-2}^\circ\text{C}$~~ approximately $2 \times 10^{-2}^\circ\text{C}$
349 and ~~$\sim 4 \cdot 10^{-2}^\circ\text{C}$, between TMI SST and tidal and non-tidal simulation~~ $4 \times 10^{-2}^\circ\text{C}$, respectively,
350 ~~indicating~~ when compared to the TMI SST. This indicates the robustness of ~~our model's~~ the
351 ~~model's~~ simulations. Over the seasonal cycle, ~~it appears that~~ the tidal ~~simulation is~~ simulations
352 ~~are~~ closer to the observations from January to March, July to September, and November to
353 December, ~~while during~~. During the rest of the year, either ~~the two~~ both simulations are equally
354 close ~~to the observations~~, or the non-tidal ~~simulation is~~ simulations are closer.

355 To gain ~~an~~ insight into our model performance along the depth, we used the mean
 356 WOA2018 climatology (2005–2017) and simulation data (salinity and temperature) for the
 357 three years 2013–2015, averaged in the same region as in Fig.3f. Figure 3g shows the
 358 Temperature-Salinity (T-S) diagram for WOA2018 and the two simulations. The data are
 359 averaged in the box as before, and we use $\sigma_{\theta}[\rho-1000]\sigma_{\theta}[\rho-1000]$ to represent the density
 360 contours, with ρ the water density. Both simulations exhibit similar patterns withas WOA2018
 361 for deeper waters, i.e., $T < 17^{\circ}\text{C}$ and $\sigma_{\theta} > 25.6 \text{ kg}\cdot\text{m}^{-3}$. However, there
 362 exist minor discrepancies for the surface layer waters, i.e., $T > 17^{\circ}\text{C}$ and $22.4 > \sigma_{\theta}$
 363 $< 25.6 \text{ kg}\cdot\text{m}^{-3}$. At that level, the tidal simulations better
 364 reproduces the T-S profile of the observations. These smallslight differences between
 365 WOA2018 observations and the two simulations, especially with the tidal
 366 simulations, further demonstrate the ability of our model to reproduce the observed
 367 water mass properties.

368 IV. Results

369 In this section, we present the influence of tides on ~~the~~ temperature, the associated
 370 processes, and the impact on the atmosphere-ocean net heat exchange. The analyses were
 371 performed on a seasonal scale between April-May-June (AMJ) and August-September-October
 372 (ASO) for the three years 2013–2015.

373 IV.1. Tide-enhanced surface cooling

374 During the first season, warm waters, which are defined as $> 27.6^{\circ}\text{C}$, dominate near the
 375 coast, especially in the middle shelf and in the south-east, and cold waters are present offshore
 376 north of 6°N (Fig.4a–c). Off the mouth of the Amazon River, water colder than 28.2°C spreads
 377 between 43°W – 51°W for TMI SST (Fig.4a) and ~~the~~ tidal simulations (Fig.4b), while
 378 warmer waters are present in the same area for the simulations without ~~the~~ tides
 379 (Fig.4c). Figures 4d–f show the SST, averaged over the ASO season. ~~The~~ TMI SST
 380 observations (Fig.4d) shows an upwelling cell represented by the extension of the 27.2°C
 381 isotherm (white dashed contour) along the slope to about 49°W – 3°N towards the north-east of
 382 the region, which forms the extension of the ACT. This extension also exists in the tidal
 383 simulations (Fig.4e), whereas $\leq 27.2^{\circ}\text{C}$ waters are not crossing 45.5°W and remain
 384 in the southern hemisphere in the simulations without ~~the~~ tides (Fig.4f). This means
 385 that waters colder than 27.2°C can only extend further into the northeast because of tides. In
 386 addition, we can note that the mean SST shows a very contrasting distribution between the two

387 seasons. There are warm waters along the shelf and cold waters offshore during the AMJ season
388 (Fig.4a-c). This is followed by warming along the Amazon plume and offshore, and an
389 upwelling cell in the south-east (Fig.4d-f).

390 The general impact of the tides, illustrated by the SST anomaly between the tidal and
391 the non-tidal ~~simulations~~simulations, is a cooling over a large part of the study area with maxima
392 up to 0.3 °C (Fig. 5a—b). For ASO, tides induce a warming (> 0.3 °C) on the shelf at the mouth
393 of the Amazon River (Fig.5b), while for AMJ it is a cooling of the same intensity (Fig.5a). That
394 difference will be further discussed. Out of the shelf, the structure of temperature anomaly ~~for~~
395 ~~each varies depending on the~~ season ~~has different spatial structures. This is,~~ probably ~~due to a~~
396 ~~different~~because of seasonal mesoscale variability ~~between the two seasons.~~

397 **IV.2. Impact of the tides inon the atmosphere-to-ocean net heat flux**

398 The atmosphere—ocean net heat flux (Q_t) reflects the balance of incoming and outgoing
399 heat fluxes across the atmosphere-ocean interface (see details on Moisan and Niiler, 1998;
400 Jayakrishnan and Babu, 2013). During AMJ, ~~the~~ tides mainly induce positive Q_t anomalies over
401 the whole domain. The average values are around 25 W.m⁻² in the plume and the Amazon
402 retroflection to the northeast and along A and B (Fig.5c). Negative SST anomalies (~0.3°C)
403 occur throughout the domain in the same location. During the ASO season, at the mouth of the
404 Amazon, there are negative Q_t anomalies but of the same magnitude as during the previous
405 season (Fig.5d). At this location, positive temperature anomalies (~0.3°C) are observed
406 (Fig.5b). Elsewhere, there are positive Q_t anomalies and negative SST anomalies. It therefore
407 appears that negative SST anomalies induce positive Q_t anomalies and vice versa. Hence, the
408 spatial structures of Q_t anomalies and SST anomalies fit ~~almost perfectly~~ together for the two
409 ~~season~~seasons. There is a strong negative correlation of 0.97 with a significance of $R^2 = 0.95$
410 for the AMJ season. ~~And roughly, and almost~~ the same ~~intensity and sign for the~~in ASO season
411 with 0.98 and 0.96, respectively for the correlation and its significance (Fig.5e). This is
412 consistent with the fact that the atmosphere and the underlying ocean are balanced. Then, the
413 SST cooling induced by upwelled cold water will try upset this balance. As a result of this, an
414 equivalent variation in the net heat flux from the atmosphere to the ocean will attempt to restore
415 it.

416 ~~The~~Figure 5f the integral over the entire domain of the net heat flux for each season and
417 for each simulation ~~is shown in Figure 5f.~~ During the AMJ season, Q_t increases from 23.85
418 TW (1 TW = 10¹² W) for the non-tidal ~~simulations~~simulations to 35.7 TW for the tidal
419 ~~simulations~~simulations, i.e., an increase of 33.2 %. That is, the tides are responsible for a third

420 of Q_t variation. This is very large compared to what is observed elsewhere in other IT hotspots
421 (e.g., 15% in Solomon Sea, Tchilibou et al., 2020). During the second season, there is a smaller
422 increase in Q_t of about 7.4% between the two simulations, i.e., from 73.03 TW ~~to 78~~to 78.83
423 TW for the non-tidal and tidal simulations respectively (Fig.5f).

424 It is also worth noting the significant difference in integrated Q_t between the two
425 seasons. The values are less than 36 TW during the AMJ season, whereas they are around twice
426 as high, > 73 TW, during the ASO season. Given that colder SST induce a stronger Q_t , these
427 higher values are likely related to the arrival of watercold waters from ACT, which forms
428 upwelling cells (Fig.4d-f) with a secondary tidal effect.

429 **IV.3. Vertical structure of Temperature along internal tides pathway**

430 To further analyze the temperature changes between ~~both~~the two simulations, we made
431 vertical sections following the path of IT radiating from sites A and B (respectively black and
432 red line in Fig.2f). Hereunder, only the transects following the pathway A ~~will be shown~~are
433 presented, since the vertical structure is similar following pathway B especially for AMJ season
434 and because some processes tend to be null along pathway B during the ASO season. The mixed
435 layer refers to a quasi-homogenous surface layer of temperature-dependent density that
436 interacts with the atmosphere (Kara et al., 2003). Its maximum depth, also known as mixed-
437 layer depth (MLD), is defined as the depth where the density increases from the surface value,
438 due to temperature change of $|\Delta T| = 0.2$ °C with constant salinity (e.g., Dong et al., 2008;
439 Varona et al., 2019).

440 Figure 6 shows the vertical sections of temperature for the two seasons following A. ~~For~~
441 theIn AMJ season, over the slope and near the coast, cold waters (< 27.6 °C) remain below the
442 surface at ~ 20 m for the tidal ~~simulations~~simulations (Fig.6a) and deeper at ~ 60 m for the non-
443 tidal ~~simulations~~simulations (not shown). ~~Then,~~The cold waters rise to the surface more than
444 400 km offshore for both simulations. ~~At theIn~~ surface layers (< 40 m), the SST~~temperature~~
445 anomaly is relatively small (\sim more than -0.3 °C, Fig.5a), ~~because the SST anomalies are likely~~
446 damped by the heat fluxes, further 8 °C at the shelf beak and less than -0.2 °C elsewhere (Fig.6b).
447 Further down (< 60 m) the water column, this anomaly becomes much larger (Fig.6b), along the
448 transect. Above that thermocline (< 120 m), the ~~simulations~~simulations with ~~the~~tides isare
449 colder by 1.2 °C from the slope, where IT are generated ~~to the open ocean and~~ following their
450 propagation pathpathway. Conversely, below the thermocline, the tidal ~~simulation~~
451 issimulations are warmer by approximately the same intensity (1.2 °C) up to ~ 300 m depth and
452 along the propagation path and down to ~ 300 m depth (Fig.6b). During thisIn AMJ season, the

453 thermocline depth is ~~~about~~ 100 m \pm \pm 15 m deep and the MLD is ~~~about~~ 40 m \pm \pm 20 m deep
454 (~~dashed white line,~~ Fig.6a). They both have a very weak slope between the coast and the open
455 ocean. Over the whole domain, the thermocline is deeper by about 15 m on average in the non-
456 tidal ~~simulations~~simulations, following the propagation paths of internal tides, on the Amazon
457 shelf and plume (Fig.6c). ~~Whilst Similarly, the~~ MLD in the non-tidal ~~simulations~~simulations is
458 deeper by ~~an average of~~approximately 10 m over the shelf, ~~~4 m~~ ~~on average~~ along IT
459 propagation paths and close to zero in the Amazon plume (Fig.6d).

460 ~~During the~~In ASO season, cold waters previously confined below the surface during the
461 previous season (AMJ) rise to the surface. These cold waters extend over the slope and up to
462 about 150 km offshore in the non-tidal ~~simulations~~simulations (not shown) and up to 250 km
463 offshore in the tidal ~~simulations~~simulations (Fig.7a). The 27.2 °C isotherm only reaches the
464 surface above the slope in the tidal ~~simulations~~simulations and remains below the surface (~30
465 m) in the non-tidal ~~simulations~~simulations (not shown). This aligns with the ~~missing~~absence of
466 that isotherm at this location in the corresponding SST map (Fig.4f). For the tidal
467 ~~simulations~~simulations, the temperature anomaly in the ASO season is smaller (~~←~~(~ -0.4 °C,
468 Fig.7b) in the surface layers (< 40 m) near the coast compared to the AMJ season (Fig.6b). In
469 contrast, during the ASO season, this cooling can drive more SST anomalies along A (-0.3 °C,
470 Fig.5b).). A stronger cooling of ~~~~~about 1.2 °C occurs deeper between 60 and 140 m depth,
471 and a warming of about 1.2 °C below, which extends less offshore than during AMJ season,
472 650 km vs. ~1000 km. ~~During this~~In ASO season, the coastward slope of the thermocline and
473 MLD becomes somewhat steeper compared to ~~the other~~AMJ season. In both simulations, there
474 is a dip of ~80 m, i.e., ~60 m offshore and ~140 m inshore, for the thermocline (~~dashed black~~
475 ~~line,~~ Fig.7a). ~~And~~, and a dip of ~40 m, i.e., ~30 m offshore and ~70 m inshore, for MLD
476 (~~dashed white line,~~ Fig.7a). Over the entire domain, ~~the~~ tides reduce the thermocline depth by
477 ~6 m on the shelf and ~12 m at the plume and far offshore along the propagation path of A
478 (Fig.7c). ~~They reduce the MLD in the tidal run~~, and they MLD by about 10 m along the shelf
479 and ~4 m along the propagation path of A (Fig.7d).

480 Between the two seasons, there is also a change in the vertical density gradient between
481 the coast and the open sea. In ~~the~~tidal ~~simulations~~simulations, during ~~the~~AMJ season, the
482 isopycnals layers are ~~tight~~thin near the coast and thicken towards the open sea (Fig.6a). This
483 means that a strong stratification is present near the coast and decreases towards the open sea.
484 In contrast, during ~~the second~~ ASO season, the isopycnals layers are thicker near the coast and
485 tight offshore (Fig.7a). As the result of this, the stratification is weaker inshore than offshore.

486 This clearly highlights a seasonality in the vertical density gradient profile in agreement with
487 Tchilibou et al. (2022). Note that this behavior also appears in the [simulations](#)
488 without ~~the~~ tides (not shown). The transects of the temperature anomaly, [Fig. 6b and 7b](#), show
489 that ~~the~~ tides influence the temperature in the ocean from the surface to the deep layers, with a
490 greater effect on the first ~~300~~[three hundred](#) meters. One question we address in this paper is to
491 better understand what processes are at work that explain these temperature changes.

492 **IV.4. What are the processes involved?**

493 To explain the observed surface and water column temperature changes, we computed
494 and analyzed the terms of the heat balance equation (see Section II.3.2, Equation 6) for both
495 seasons (AMJ and ASO).

496 **IV.4.1. Vertical diffusion of Temperature**

497 Figure 8 shows the vertical temperature diffusion tendency (ZDF). ZDF is averaged
498 between 2–20 m, i.e., within the mixed-layer. For the AMJ season, ZDF in the tidal
499 [simulations](#) (Fig. 8a) shows a negative trend (i.e., cooling) in the whole domain. The
500 maximum values (~~≈ -0.4~~ [\$> 0.4\$](#) $^{\circ}\text{C}\cdot\text{day}^{-1}$) are located along the slope where IT are
501 generated and on their propagation path. There is a larger horizontal extent along A of ~ 700 km
502 from the coasts compared to B, where it is ~ 300 km from the coasts. Elsewhere, ~~it remains very~~
503 ~~low,~~ [\$> -0.1\$](#) $^{\circ}\text{C}\cdot\text{day}^{-1}$. ZDF is weak (> -0.1 $^{\circ}\text{C}\cdot\text{day}^{-1}$). For the non-tidal [simulations](#)
504 (Fig. 8b), ~~the~~ ZDF is ~~very~~ weak over the entire domain (~~≈ -0.1~~ $^{\circ}\text{C}\cdot\text{day}^{-1}$). ~~For~~
505 ~~the~~ (> -0.1 $^{\circ}\text{C}\cdot\text{day}^{-1}$). In ASO season, the tidal [simulations](#) (Fig. 8c) ~~show~~[show](#)
506 a decrease of the ZDF near the coast (< 100 km) and a strengthening offshore along A compared
507 to the previous season, but with the same cooling trend (~~≈ -0.4~~ $^{\circ}\text{C}\cdot\text{day}^{-1}$). Along B, it tends to be null, both at the coast and offshore (Fig. 8c). In addition, the mesoscale
508 circulation and eddy activity intensify during this season. To the northeast, [approximately](#)
509 between 4°N – 8°N , and 47°W – 53°W , there is a cooling on the shelf of ~~-0.3~~
510 [\$\sim 0.3\$](#) $^{\circ}\text{C}\cdot\text{day}^{-1}$ with eddy-like patterns in the tidal [simulations](#) (Fig. 8c). The
511 processes by which these features might arise ~~will be~~ discussed in more details in
512 [Section](#) V. Unsurprisingly, ZDF is ~~very~~ weak ~~elsewhere~~[everywhere](#) for the non-tidal
513 [simulations](#) (Fig. 8d). [Internal tides](#) IT are the dominant driver of vertical diffusion of
514 temperature along the shelf break and offshore, while the mixing induced by barotropic tides
515 ~~could~~ prevail on the shelf.

517 On the vertical following A, there are opposite sign ZDF values, with mean magnitude
518 of $\sim |0.4| \text{ } ^\circ\text{C}\cdot\text{day}^{-1}$. These values are centered around the thermocline for the
519 ~~simulations~~ with tides in the two seasons AMJ and ASO (respectively Fig.8e and 8f).
520 There is a cooling trend above the thermocline and a warming trend below. The average vertical
521 extent is up to ~ 350 m depth for the maximum values but exceeds 500 m depth for the low
522 values ($\ll 0.1 \text{ } ^\circ\text{C}\cdot\text{day}^{-1}$). As for the horizontal averages (Fig.9a8a and 9e8c),
523 from one season to another there is a weakening of ZDF above the slope and a strengthening
524 offshore, Fig.8e and 8f, for AMJ and ASO, respectively. Furthermore, offshore ZDF maxima
525 ~~seem to be~~ discontinuous and spaced of about 140–160 km during the AMJ season (Fig.8e)
526 but are more continuous for the ASO season (Fig.8f). For the non-tidal ~~simulations~~,
527 the mean ZDF tends to be null in the ocean interior but remains quite large (≈ -0.2
528 $\text{ } ^\circ\text{C}\cdot\text{day}^{-1}$) ($> -0.2 \text{ } ^\circ\text{C}\cdot\text{day}^{-1}$) in the thin surface layer during the two seasons (Fig.8g–h).

529 Furthermore, it is worth to noting that along IT propagation's pathway, the maximum
530 of the ZDF follows the maxima of the baroclinic tidal energy dissipation (~~color shading in~~
531 Fig.2f). ~~Thus, This proves that~~ the dissipation of IT causes vertical mixing that enhances ~~the SST~~
532 ~~cooling of the sea surface.~~ In addition, this temperature diffusion contributes to greater
533 subsurface cooling within the mixed-layer and warming in the deeper layers beneath the
534 thermocline.

535 The seasonality of the stratification, highlighted above, could explain why the ZDF is
536 stronger along the slope and the near-coastal pathway B during the AMJ season (Fig.8a and
537 8e), and why ~~in ASO season~~ ZDF is weaker along the slope, close to zero following B, and
538 reinforce offshore of A ~~during the ASO season~~ (Fig.8c and 8f). Previous studies have shown
539 that stratification influences the generation of internal tides and controls their modal
540 distribution. Here we show that stratification also plays a role on the fate of these internal tides,
541 in this case on their dissipation. The stratification could determine where IT dissipate their
542 energy in the water column, as mentioned by de Lavergne et al. (2020).

543 IV.4.2. Advection of temperature

544 The vertical (z-ADV) and the horizontal (h-ADV) terms of the temperature advection
545 tendency are averaged in the same depth-range as above for the two seasons.

546 IV.4.2.a Vertical advection of Temperature

547 Tides fail to generate vertical temperature advection within surface layers. As expected,
548 z-ADV is almost null ~~in these surface layers~~ throughout the region in that depth-range (Fig.9a-

549 ~~–d). For Nevertheless, for~~ both seasons, ~~some weak~~ there are extreme values are located in the
 550 northwest on the plateau between 54°W–50°W and 3°N–~~36°N~~ and are for with the same
 551 intensity between in the two simulations ~~with and without tides. This result suggests that,~~
 552 ~~overall, the tides fail to generate vertical temperature advection within these surface layers,~~
 553 ~~but~~ ($<0.3 \text{ }^\circ\text{C}\cdot\text{day}^{-1}$). But deeper, ~~z-ADV become higher. Vertical~~ vertical sections (Fig.9a–h)
 554 show an intensification of z-ADV of about $\pm 0.8 \text{ }^\circ\text{C}\cdot\text{day}^{-1}$ located below the MLD
 555 and seems to be centered around the thermocline, with a vertical extension from 20–200 m
 556 depth. z-ADV is stronger in tidal ~~simulations~~ simulations during both seasons (Fig.9e–f,) and
 557 ~~mainly~~ presents sparse extrema offshore ($>300 \text{ km}$) for the non-tidal ~~simulations~~ simulations
 558 (Fig.9g–h). For the ~~simulations~~ simulations with ~~the~~ tides, z-ADV appears to be ~~rather~~
 559 dominated by a cooling trend, with a marked hotspot on the slope followed by other hotspots
 560 offshore. These extreme values are spaced about 120–150 km apart, i.e., a mode-1 wavelength
 561 as for the baroclinic tidal energy dissipation (Fig.2f). Note that for both simulations (Fig.10e–
 562 ~~9e–h~~), the extreme values are located within the narrow density (σ_θ) contours [~~23.8–26.2 kg·m⁻³~~
 563 $23.8\text{--}26.2 \text{ kg}\cdot\text{m}^{-3}$], i.e., within the pycnocline. The location of the extreme values of z-ADV
 564 at the shelf break and along IT ~~propagation's pathway~~ propagation pathways and its negative
 565 sign suggest that the diffusive part of the advection scheme ~~might be the dominant process~~
 566 ~~compared to nonlinear effects.~~ may account significantly in z-ADV.

567 IV.4.2.b Horizontal advection of temperature

568 Horizontal advection of temperature (h-ADV) is defined as the sum of the zonal (x-
 569 ADV) and meridional (y-ADV) terms of temperature advection tendency. As for z-ADV, the
 570 mean of h-ADV tends to be null over the entire domain in the surface layers for both seasons
 571 in both simulations (Fig.10a–d). Nevertheless, ~~some weak~~ extreme values are extremums exist
 572 in the northwest of the plateau between 54°W–50°W and 3°N–~~37°N~~, ~~that. These~~ intensify
 573 during the ASO season in both simulations, ~~~±0.2 °C·day⁻¹, Fig.~ ±0.2 °C·day⁻¹, Figure 10c~~
 574 and 10d for the tidal and non-tidal simulations, respectively. ~~During~~ In AMJ season, h-ADV is
 575 slightly stronger, ~~~0.1 °C·day⁻¹, ~0.1 °C·day⁻¹,~~ around sites A and B in the tidal
 576 ~~simulations~~ simulations (Fig.10a), which appears to be related to IT generated along the slope.
 577 ~~On the other hand, the small difference~~ However, there is a slight distinction between the two
 578 simulations in the surface layers ~~shows, suggesting that the tides hardly generate~~ have a minimal
 579 effect on h-ADV. ~~Then, as expected. Consequently,~~ h-ADV ~~hardly has a negligible~~
 580 on the cold-water tongue observed ~~over~~ in the surface SST during the ASO season (Fig.4d–f).

581 Along the vertical following A, h-ADV maxima ~~remain essentially are~~ confined below
582 the mixed-layer depth, ~~with much~~. The tidal simulations (Fig.10e-f) exhibit ~~significantly~~ more
583 intense values ~~in the tidal simulation (Fig.10e-f)~~ compared to the non-tidal
584 ~~simulations~~ (Fig.10g-h). h-ADV contributes to both warming and cooling of the
585 temperature, ~~with a magnitude of ± 0.4 °C.day⁻¹~~ ~~about ± 0.4 °C.day⁻¹~~, ~~extending~~
586 to ~~more than~~ ~~over~~ 500 km offshore. ~~During~~ ~~In~~ both seasons, the average vertical extension lies
587 between the surface and 400 m depth for the tidal ~~simulations~~ ~~simulations~~, and ~~a little less~~
588 ~~extended~~ between 20-300 m depth for the non-tidal ~~simulation~~. ~~As for~~ ~~simulations~~. Similarly
589 ~~to z-ADV~~, h-ADV is ~~also~~ stronger within the pycnocline. ~~For~~ ~~In~~ the tidal ~~simulation~~, ~~there~~
590 ~~is~~ ~~simulations~~, a warming ~~effect is observed~~ above the slope (~~0.4 °C.day⁻¹~~)(0.4 °C.day⁻¹),
591 reaching the surface in both seasons. This vertical excursion is ~~also~~ ~~observed elsewhere~~ for ZDF
592 and z-ADV, and it is ~~probably~~ a marker of local dissipation of IT at their generation ~~site~~. ~~This~~
593 ~~local dissipation clearly affects both advection and vertical diffusion of the temperature but~~
594 ~~there are very low values along the slope when averaging h-ADV or z-ADV between 2-20 m~~
595 ~~and much more strong values for the ZDF. This means~~ ~~sites~~. It is noteworthy that the energy
596 ~~dissipated by internal tides is mostly transferred to mixing. In addition, unlike ZDF and z-ADV,~~
597 ~~the (horizontal) location of h-ADV maxima mismatch IT does not coincide with the~~
598 ~~dissipation hotspots of IT, in contrast of ZDF and z-ADV.~~

599 IV.4.3. Heat budget balance

600 From the sections above, it is evident that IT-induced mixing within the mixed layer
601 emerges as the primary driver among the ocean's internal processes in explaining changes in
602 SST. However, below MLD, advective processes play a more significant role in structuring
603 temperature. Figure 10 shows presents the average of the terms of the heat balance equation
604 averaged below the MLD Equation 6 below MLD within the depth range of 60-400 m. The
605 analysis focuses on a specific region with latitude and longitude ranging between 60 and 400
606 m depth in a region around the IT trajectories emanating from A 0°N-6°N and B between 40°W-
607 48°W and 0°N-6°N, respectively. This region includes the two main IT paths, as well as a
608 portion of the along-coast upwelling region. During the AMJ season, advection (ADV)
609 dominates is the dominant process over diffusion terms for in both tidal (Fig.11a) and non-tidal
610 (Fig.11b) simulations, while during. However, in the ASO season, advection dominates ADV
611 only dominate in tidal simulations (Fig.11c) and), while ZDF dominates in non-tidal
612 simulations (Fig.11d). We show here that advection terms dominate under the MLD, while from
613 the two sections above, in the tidal simulation, ZDF dominates the advection terms at

614 It therefore appears that ADV only have a considerable influence on temperature below
615 MLD, contrasting with the study of Neto and da Silva (2014), which identify ADV as the
616 primary driver causing along-coast SST cooling. However, we can assume that advection and
617 mixing are interconnected. In other words, the water masses that are advected below MLD may
618 undergo mixing within the surface and within the mixed layer and is the main contributor within
619 the layers due to the overall mixing occurring throughout the water column. Additionally, it is
620 worth mentioning that in our simulations, Asselin has a negligible impact on temperature.
621 Conversely, Forcing term does impact the temperature within the surface layers. However, we
622 have not discussed this aspect in our analysis as our primary focus was on understanding the
623 internal processes of the ocean processes to explain SST changes. That vertical profile is
624 probably the case in the real ocean since the tidal simulation is more representative of reality.

625 **V. Discussion**

626 **V.1. On the role of advection in coastal upwelling**

627 To explain the cooling of the SST at the surface, Neto and da Silva (2014) indicated that
628 the steady flow of the NBC induces northward transport of water masses. This transport is in
629 turn offset by a vertical advection of cool water towards the surface. We demonstrate with our
630 model that the vertical advection hardly modifies the SST. But it is rather working below the
631 mixed layer (Fig.9e-h). The tides induced vertical diffusion (mixing) extends from the mixed
632 layer to deeper layers (Fig.8e-f). It is possible that the vertical mixing upwells to the surface the
633 water masses that are advected into the layers below the mixed layer. The temperature change
634 at the surface and within the mixed layer can then be influenced to first order by (i) the vertical
635 diffusion of temperature and (ii) a cross effect between the latter and the advection (vertical and
636 horizontal) of temperature that mainly takes place below MLD.

637 **V.2. The mode-1 wavelength in the vertical terms of the heat** 638 **budget equation**

639 Along the vertical and towardtowards the open ocean, both ZDF and z-ADV tendencies are
640 found to have exhibit a wave-like structure. For z-ADV, with patches that are spaced apart by
641 about 120–150 km and 140–160 km for the AMJ and ASO seasons respectively. Whilst for z-
642 ADV, this 120–160 km typical of mode-1 wavelength is about 140–160 km. However, during
643 the AMJASO season and, this pattern is not observed for ZDF. Instead, ZDF values appear
644 more continuous patches for the ASO season. The wavelength ranges found in heat budget

645 terms are slightly wider (+10–20 km, for z-ADV in ASO season and for ZDF) than the purely
646 dynamic tidal coherent wavelength (~120–150 km, see section III.1). The difference can be
647 understood as the effect along the transect, likely due to additional mixing caused by the
648 breaking of incoherent IT that are not captured by the harmonic analysis because they are
649 deviated or diffracted by the currents and eddies, and for which dissipation occurs around where
650 coherent IT dissipate. Hence, the total (coherent + incoherent) dissipation pattern of IT could
651 be wider than in Figure 2f. When integrating heat budget terms over the season, this cumulative
652 effect is considered and therefore leads to diffusive patterns and wider wavelength. This
653 diffusive effect intensifies during the ASO season when both background circulation
654 and eddy activity increase.

655 Recently that season. Furthermore, de Macedo et al. (2023) have recently provided a detailed
656 description of internal solitary waves (ISW) in this the same region from based on remote
657 sensing data. These ISWs originate from instabilities and energy loss or dissipation of IT
658 radiating from the slope, mainly primarily along the pathways A and B (Magalhaes et al., 2016).
659 The first have shown study demonstrated that the inter-packet distance of ISWs corresponds
660 to the mode-1 wavelength. Interestingly, the positions of IT dissipation and deeper heat budget
661 term hotspots, as well as z-ADV patches of our simulations are colocalized horizontally in both
662 seasons and ZDF patches, especially during the AMJ season, in our model align with the
663 observed ISW packets occurrences of ISWs (refer to Figure 2 in their study). This
664 means provides evidence that our model well accurately reproduces the location of IT
665 dissipation.

666 **V.3. Tidal impact at 2. Temperature changes over the mouth of the Amazon** 667 **River and on the southern shelf: two main competitive processes**

668 In the simulation without the tides, there is a strong along-coast current exiting
669 northwesterly the mouth of the Amazon River (e.g., Ruault et al., 2020) with an average
670 intensity $> 0.5 \text{ m.s}^{-1}$ lower than 0.5 m.s^{-1} in the first 50 meters for both seasons (Fig.12a–b).
671 When including the tides in the model, the latter study showed that there is an increase in the
672 vertical mixing in the water column due to stratified-shear flow instability, which weakens and
673 deflects the along-coast current north-eastwards at the mouth of the Amazon River (Fig.12c–
674 d) and favours favors cross-shore export of water. We can therefore establish that there are at
675 least two processes at work: (i) vertical mixing and (ii) horizontal transport, backed respectively
676 by ZDF and h-ADV. We then looked at the latter two processes along the vertical following
677 the cross-shore transect (C-S) defined in Figure 10b10c. Hereinafter, “inner mouth” refers to

678 the part of the transect ~~before~~ within 200 km from the shore, whereas “outer shelf” refers to the
679 part beyond.

680 During the AMJ season, in the inner mouth, ~~river of the region, the~~ flow ~~dominates and of~~
681 the river becomes dominant. The tide-induced vertical mixing in the narrow water column ~~leads~~
682 ~~to results in the~~ warming and deepening of the thermocline (Fig. 13a–b). ~~On~~ Conversely, on the
683 outer shelf, this mixing occurs in the thicker water column ~~leads, leading~~ to cooling above the
684 thermocline and warming below (Fig. 13a), ~~which in turn~~. This pattern extends across the shelf
685 and along the pathways of ~~IT~~ internal tides, as shown in ~~section~~ Section IV.4.1 (~~see refer to~~ Fig. 8a
686 and 8e). ~~At the same time, the SST on the shelf is somewhat homogeneous (see Fig. 4a–c) and~~
687 ~~solar radiation is lower than $190 \text{ W}\cdot\text{m}^{-2}$ (not shown). As a~~ In this season, the weaker circulation
688 may result, ~~waters of similar temperature are advected horizontally, i.e., h- in low values of h-~~
689 ADV is low (Fig. 13b). ~~Thus, for~~ Therefore, during the first season, ~~vertical mixing seems to be~~
690 the dominant process ~~explaining that explains~~ the average negative SST anomaly ~~on the~~
691 plateau over the shelf appears to be vertical mixing.

692 ~~For~~ During the second season, there is a significant increase in solar radiation on the shelf
693 ~~rose sharply,~~ with an average value of ~~$60 \text{ W}\cdot\text{m}^{-2}$~~ $60 \text{ W}\cdot\text{m}^{-2}$, compared ~~with to~~ the previous season
694 (Fig. 13c) ~~and~~. Additionally, the average depth of the thermocline ~~deepens~~ deepened further
695 offshore (Fig. 13d and 13e). In this season, mixing ~~leads~~ processes lead to warming in the thin
696 surface layer (~~←,~~ specifically in depths less than 2m- (Fig. 13d). ~~The~~ NBC is stronger ~~and can~~
697 ~~influence,~~ resulting in an increase of the transport over the shelf (Prestes et al., 2018) ~~and~~. It
698 is also important to consider the small mean tidal residual transport ~~should also be considered~~
699 (Bessières et al., 2008). ~~The region is,~~ which reinforces the stronger current transport. These
700 factors contribute to a more dynamic region and ~~waters of distinct temperatures are advected~~
701 ~~over the shelf~~ an increase in h-ADV (Fig. 13e). Consequently, ~~h-ADV is stronger and positive~~
702 ~~(Fig. 13e) and then~~ ADV plays a ~~greater~~ significant role in ~~the fate of~~ determining SST on the
703 shelf. For this season, ~~ZDF and h-ADV add to explain~~ the combination of these two processes
704 explains the observed positive SST anomaly ~~on the shelf. In addition,~~

705 Additionally, from the AMJ to ASO, ~~we noted the seasons, there is a notable~~ deepening of
706 the thermocline depth on the outer shelf. This ~~was~~ observation has previously been highlighted
707 by Silva et al. (2005) from REVIZEE (Recursos Vivos da Zona Econômica Exclusiva–)
708 campaign data ~~and is a,~~ further ~~contribution to the validation~~ validating of our simulations.

V.43. Mixing in the NBC retroflection area

To the north-west of the domain [3°N – 9°N and 53°W – 45°W], in the surface layers (2–20m), eddy-like or circular patterns exist in ZDF during the ASO season for the simulation including tides (Fig.8c). NBC intensifies and retroflects, and strong eddy activity takes place there during ASO. We can assume that this intense mesoscale activity influences the mixing and subsequent temperature diffusion. However, it is not yet clear how these mesoscale features produce mixing. Fronts exist in such region and are associated with high horizontal temperature gradient (∇T) and significant vertical mixing (see Chapman et al., 2020). We therefore examined the mean ∇T in the same depth range (2–20m) as ZDF (Fig.8a–d2–20 m). During the AMJ season, ∇T is on average equal to $4 \times 10^{-2} \text{ }^{\circ}\text{C}/10 \text{ km}$. As expected, it does not reveal any circular fronts for the two simulations (Fig.14a–b) since mesoscale activity is low. ∇T increases during the ASO season [$> 5 \times 10^{-2} \text{ }^{\circ}\text{C}/10 \text{ km}$] in the north-west and exhibits circular and filamentary fronts in both the non-tidal simulations (Fig.14c) and tidal (Fig.14d) simulations. Therefore, one would expect to see the same circular patterns in the ZDF for both simulations, this is not actually the case (see Fig.8c and 8d). Another hypothesis is that these circular patterns could be originated from the interaction between IT and near-inertial oscillations, which can enhance mixing and vertical transport processes in the ocean. But quantifying this interaction requires further analysis and is beyond the scope of this study.

VI. Summary

In this paper, we used twin oceanic simulations (with and without tides) from a realistic model to investigate the influence of internal tidal waves (IT) on temperature and associated processes. The impact on the atmosphere to ocean net heat fluxes is also covered.

The AMAZON36 through twin simulations including or excluding tidal forcing, using the NEMO model configuration ~~called~~ AMAZON36. Our tidal simulations accurately reproduce the generation of IT from two most energetic sites A and B, in good agreement with previous studies. The model well reproduces their local, on-shelf, and offshore and dissipation with two beams of mode-1 propagation (120–150 km). This dissipation occurs less than 300 km from IT. When comparing the slope. Then, we assess the ability of the model to reproduce temperature structure. The simulations including tides to observations, there is a better

740 agreement ~~with in sea surface temperature (SST observations)~~ and ~~better reproduce~~ water mass
741 properties along the vertical.

742 ~~Our analyses were based on~~ We then focus our analysis on a ~~three years-year period~~
743 (2013–2015) ~~of data averaged over and~~ two seasons, AMJ (~~April-May-June~~) and ASO
744 (~~August-September-October~~). ~~That are highly contrasted in terms of, which have contrasting~~
745 stratification, ~~background~~ circulation and ~~EKE-IT~~ activity.

746 Results ~~show~~ demonstrate that ~~for both seasons, the tides create SST~~ cause a cooling
747 ~~effect in SST~~ of about 0.3°C in the ~~plume of the~~ Amazon offshore ~~plume~~ and along the paths
748 of ~~internal tides. During IT~~ in both seasons. ~~In the ASO, the cold waters of the ACT enter our~~
749 ~~domain along the coast and are affected by the tides. This enhances that season particularly,~~
750 ~~tides enhance~~ seasonal upwelling ~~and leads, leading~~ to cooler SST. Over the Amazon shelf, ~~the~~
751 tides induce ~~the same magnitude~~ cooling in AMJ and ~~in turn induce an opposite anomaly~~
752 (~~warming~~) in ASO. These cooling/warming ~~are responsible in the same location for an~~
753 ~~increase/decrease in patterns over the region affect~~ the net heat flux ~~from between~~ the
754 atmosphere ~~to and~~ the ocean (Q_t). ~~However, As~~ the ~~result, there is an~~ overall ~~effect of the tides~~
755 ~~is an~~ increase of Q_t , ~~which lies between [from 33.2% -7.4%] from in~~ AMJ to ~~7.4% in~~ ASO
756 ~~and is larger than in other regions. When increasing the atmosphere to ocean net heat flux,~~
757 ~~Changes in Q_t~~ in such large atmospheric convection ~~region, marked by the ITCZ, the~~
758 ~~tides regions~~ can reduce ~~the~~ cloud convection into the atmosphere (Koch-Larrouy et al., 2010).
759 Therefore, ~~this understanding changes in~~ tidal ~~effect on the climate might have a key importance~~
760 ~~for the future, taking the activity become crucial to better assess~~ climate change ~~into account~~
761 (Yadidya and Rao, 2022).

762 In the subsurface, ~~above in both seasons,~~ the ~~thermocline (<120 m), the findings reveal~~
763 ~~that~~ tides induce a stronger cooling (-1.2°C) ~~than at the surface. And an associated above the~~
764 ~~thermocline (<120m) and~~ warming ~~of the same below (> 120–300m), with a mean~~ magnitude
765 ~~under the thermocline (>120–300 m). We analyzed the terms of about 1.2°C .~~

766 ~~The analysis~~ of the heat budget equation ~~to identify to processes that modify the~~
767 ~~temperature. We found that the vertical diffusion of temperature (ZDF) is mainly caused by~~
768 ~~the dissipation of the tides. Horizontal (h-ADV) and vertical (z-ADV) advection can be driven~~
769 ~~by non-tidal processes but increase when including the tides in the model.~~

770 ~~Over the shelf, barotropic tidal mixing increases ZDF (>|0.4| $^{\circ}\text{C}\cdot\text{day}^{-1}$) and explain the~~
771 ~~cooling of the water column in AMJ season. During the second season, it combines with h-~~
772 ~~ADV and to cause a warming. Off the shelf, the (baroclinic) mixing takes place from the slope~~

773 to about 700 km following the path A, and 300 km following the path B. That mixing induces
774 ZDF with values of about $0.4\text{ }^{\circ}\text{C}\cdot\text{day}^{-1}$, which is the main process in the upper layer
775 ~~above reveals that within~~ the mixed layer ~~but could combine with advection terms (z-ADV and~~
776 ~~h-ADV) to explain~~, the temperature changes are primarily influenced by the vertical diffusion
777 of temperature (ZDF). This diffusion is driven by diapycnal mixing, which results from
778 barotropic tide bottom friction over the shallow shelf and the breaking of IT at their generation
779 sites and along their propagation pathways. It is noteworthy that the ZDF values are highest in
780 these latter two areas. In deeper layers below the mixed layer. Some, ZDF combines with
781 vertical and horizontal advection terms (z-ADV and h-ADV) to explain temperature changes.
782 Notably, ZDF and z-ADV patches ~~are colocalized coincide~~ with dissipation hotspots ~~along the~~
783 trajectory of IT. energy.

784 This study highlights the key role importance of internal tides in creating the intensified
785 mixing which is important of IT for temperature structure. ~~Other analysis we performed with We~~
786 focused hereabove on describing the impacts of tides in temperature on a seasonal scale.
787 However, a companion paper will then analyze the variability of temperature at tidal and
788 subtidal scales using our simulations ~~show that this mixing can also impact salinity. and remote~~
789 sensing data.

790 Furthermore, ~~they might be seen as a other analysis from our simulations revealed a~~
791 significant impact on salinity. In addition, IT was reported to be a source of nutrient uptake at
792 tidal frequency and can have an and impact ~~on~~ the spatial distribution of phytoplankton and
793 zooplankton, and therefore on the entire food chain (Sharples et al., 2007, 2009; Xu et al., 2020).
794 ~~These other impacts can be studied through a combined model in situ data approach. Long-~~
795 ~~term PIRATA (Prediction and Research moored Array in the Tropical Atlantic) mooring data~~
796 ~~are available for this goal (Bourlès et al., 2019). In addition, recently in late 2021, the AMAZOn~~
797 ~~MIXing (“AMAZOMIX”) campaign took place in this region. Among other things, this~~
798 ~~campaign was dedicated to internal tides. It provided a huge set of data, with the aim of~~
799 ~~understanding their impact on marine ecosystems (see details in [https://en.ird.fr/amazomix-](https://en.ird.fr/amazomix-campaign-impact-physical-processes-marine-ecosystem-mouth-amazon)~~
800 ~~[campaign-impact-physical-processes-marine-ecosystem-mouth-amazon](https://en.ird.fr/amazomix-campaign-impact-physical-processes-marine-ecosystem-mouth-amazon)).~~ In the meantime, a
801 ~~coupled physical/biogeochemistry simulation (NEMO/PISCES) is being analyzed and will~~
802 ~~begin to answer these crucial questions. Ongoing investigations is conducted to assess the~~
803 impacts of tides on marine ecosystems using a combined approach including:

804 ~~Finally, we focused hereabove on describing the impacts of tides on a seasonal scale. A~~
805 ~~companion paper will then analyze the variability of temperature at tidal and subtidal scales~~
806 ~~using our model simulations and two observational data.~~

- 807
- 808 1- the new designed coupled physical/biogeochemistry simulations from NEMO/PISCES
809 called *AMAZON36-BIO* and;
 - 810 2- *in situ* data, consisting of long-term PIRATA mooring data (Bourles et al., 2019) and
811 the recent Amazon mixing campaign (AMAZOMIX, Bertrand et al., 2021).

812

813 ***Data availability statements***

814 ~~._~~The ~~2020's~~2020 release of GEBCO bathymetry is publicly available online through:
815 https://www.gebco.net/data_and_products/gridded_bathymetry_data/gebco_2020/. The TMI
816 SST v7.1 data are publicly available online from the REMSS platform:
817 <https://www.remss.com/missions/tmi/>, ~~was accessed on~~last access: 27 June 2022. WOA2018
818 climatology is publicly available online at: [https://www.ncei.noaa.gov/access/world-ocean-](https://www.ncei.noaa.gov/access/world-ocean-atlas-2018/)
819 [atlas-2018/](https://www.ncei.noaa.gov/access/world-ocean-atlas-2018/), ~~was accessed on~~last access: 27 June 2022. The model simulations are available
820 upon request by contacting the corresponding author.

821 *Authors contributions.* AKL: Funding acquisition; FA, AKL, and ID: Conceptualization and
822 methodology; GM and FA, with assistance from JC and AKL: Numerical simulations; Formal
823 analysis: FA with interactions from all co-authors; Preparation of the manuscript; FA with
824 contributions from all co-authors.

825 ~~Funding acquisition, AKL; Conceptualization and methodology, FA, AKL and ID.~~
826 ~~Numerical simulations, GM and FA. Formal analysis, FA; FA prepared the paper with~~
827 ~~contribution from all co-authors.~~

828 ***Competing interests***

829 ~~._~~The authors declare that they have no conflict of interest.

830

831 *Disclaimer. Publisher's note:* Copernicus Publications remains neutral regarding jurisdictional
832 claims in published maps and institutional affiliations.

834 [Acknowledgements](#). The Authors would like to thank the Remote Sensing System (REMSS) for
835 providing TMI SST datasets, and the NASA’s National Center for Environmental Information
836 (NCEI) for providing World Ocean Atlas 2018 (WOA2018) data. The Authors would like to
837 thank the Editorial team for their availability and are grateful to the two Reviewers Clément
838 Vic and Nicolas Grisouard for their valuable comments, which helped to improve the quality
839 of the present work.

841 **Funding**

842 This work is part of the PhD Thesis of FA, cofounded by Institut de Recherche pour le
843 Développement (IRD) and Mercator Ocean International (MOi), under the [supervisionco-](#)
844 [advising](#) of AKL and ID. The numerical simulations were founded by [CNES/CNRS/CNES/IRD](#)
845 via the projects A0080111357 and A0130111357 and were performed thank to “Jean-Zay”, the
846 CNRS/GENCI/IDRIS platform for modelling and computing.

847 **Acknowledgments**

848 ~~The authors would like to thank the Editorial team for their availability,~~
849 ~~Review statement. This paper was edited by Rob Hall and the two reviewers reviewed by~~
850 Clément Vic and Nicolas ~~Grissouard for their valuable comments, which enhanced the quality~~
851 ~~of the present work~~[Grisouard](#).

853 **References**

- 854 Aguedjou, H.M.A., Chaigneau, A., Dadou, I., Morel, Y., Pegliasco, C., Da-Allada, C.Y.,
855 Baloïtcha, E., [2021](#).: What Can We Learn From Observed Temperature and Salinity
856 Isopycnal Anomalies at Eddy Generation Sites? Application in the Tropical Atlantic
857 Ocean. *J. Geophys. Res. Oceans*, 126, [e2021JC017630](#):[JC017630](#),
858 <https://doi.org/10.1029/2021JC017630>, [2021](#).
- 859 Aguedjou, H.M.A., Dadou, I., Chaigneau, A., Morel, Y., Alory, G., [2019](#).: Eddies in the
860 Tropical Atlantic Ocean and Their Seasonal Variability. *Geophys. Res. Lett.*, 46,
861 12156–12164. <https://doi.org/10.1029/2019GL083925>, [2019](#).
- 862 Archer, D., Martin, P., Buffett, B., Brovkin, V., Rahmstorf, S., Ganopolski, A., [2004](#).: The
863 importance of ocean temperature to global biogeochemistry. *Earth Planet. Sci. Lett.*,
864 222, 333–348. <https://doi.org/10.1016/j.epsl.2004.03.011>, [2004](#).
- 865 Baines, P.G., [1982](#).: On internal tide generation models. *Deep Sea Res. Part Oceanogr. Res.*
866 *Pap.*, 29, 307–338. [https://doi.org/10.1016/0198-0149\(82\)90098-X](https://doi.org/10.1016/0198-0149(82)90098-X), [1982](#).
- 867 Barbot, S., Lyard, F., Tchilibou, M., Carrere, L., [2021](#).: Background stratification impacts on
868 internal tide generation and abyssal propagation in the western equatorial Atlantic and
869 the Bay of Biscay. *Ocean Sci.*, 17, 1563–1583. [https://doi.org/10.5194/os-17-1563-](https://doi.org/10.5194/os-17-1563-2021)
870 [2021](#), [2021](#).

871 Barton, E.D., Inall, M.E., Sherwin, T.J., Torres, R., 2001.: Vertical structure, turbulent mixing
872 and fluxes during Lagrangian observations of an upwelling filament system off
873 Northwest Iberia. *Prog. Oceanogr.*, Lagrangian studies of the Iberian upwelling
874 system, 51, 249–267. [https://doi.org/10.1016/S0079-6611\(01\)00069-6](https://doi.org/10.1016/S0079-6611(01)00069-6), 2001.

875 Beardsley, R.C., Candela, J., Limeburner, R., Geyer, W.R., Lentz, S.J., Castro, B.M.,
876 Cacchione, D., Carneiro, N., 1995.: The M2 tide on the Amazon Shelf. *J. Geophys.*
877 *Res. Oceans*, 100, 2283–2319. <https://doi.org/10.1029/94JC01688>, 1995.

878 Bertrand, A., De Saint Leger, E., and Koch-Larrouy, A.: AMAZOMIX 2021, French
879 Oceanographic Cruises, <https://doi.org/10.17600/18001364>, 2021.

880 Bessières, L., 2007.: Impact des marées sur la circulation générale océanique dans une
881 perspective climatique (phdthesis). Ph.D Thesis, *Océan Atmosphère*, Université Paul
882 Sabatier - Toulouse III, France, 179pp., 2007.

883 Bessières, L., Madec, G., Lyard, F., 2008.: Global tidal residual mean circulation: Does it affect
884 a climate OGCM?. *Geophys. Res. Lett.*, 35(3), L03609,
885 <https://doi.org/10.1029/2007GL032644>, 2008.

886 ~~Bourlès~~ Bourles, B., Molinari, R.L., Johns, E., Wilson, W.D., Leaman, K.D.: Upper layer
887 currents in the western tropical North Atlantic (1989–1991), *J. Geophys. Res. Oceans*,
888 104, 1361–1375, <https://doi.org/10.1029/1998JC900025>, 1999.

889 Bourles, B., Araujo, M., McPhaden, M.J., Brandt, P., Foltz, G.R., Lumpkin, R., Giordani, H.,
890 Hernandez, F., Lefèvre, N., Nobre, P., Campos, E., Saravanan, R., Trotte-Duhà, J.,
891 Dengler, M., Hahn, J., Hummels, R., Lübbecke, J.F., Rouault, M., Cotrim, L., Sutton,
892 A., Jochum, M., Perez, R.C., 2019.: PIRATA: A Sustained Observing System for
893 Tropical Atlantic Climate Research and Forecasting. *Earth Space Sci.*, 6, 577–616,
894 <https://doi.org/10.1029/2018EA000428>, 2019.

895 ~~Bourles, B., Molinari, R.L., Johns, E., Wilson, W.D., Leaman, K.D., 1999. Upper layer currents~~
896 ~~in the western tropical North Atlantic (1989–1991). *J. Geophys. Res. Oceans* 104, 1361–~~
897 ~~1375. <https://doi.org/10.1029/1998JC900025>~~

898 Buijsman, M.C., Arbic, B.K., Richman, J.G., Shriver, J.F., Wallcraft, A.J., Zamudio, L., 2017.:
899 Semidiurnal internal tide incoherence in the equatorial Pacific. *J. Geophys. Res.*
900 *Oceans*, 122, 5286–5305. <https://doi.org/10.1002/2016JC012590>, 2017.

901 ~~C., Le Provost, Florent, Lyard, 1997. Energetics of the M2 barotropic ocean tides: an estimate~~
902 ~~of bottom friction dissipation from a hydrodynamic model — *ScienceDirect. Prog.*~~
903 ~~*Oceanogr.* 37–52.~~

904 Chapman, C.C., Lea, M.-A., Meyer, A., Sallée, J.-B., Hindell, M., 2020.: Defining Southern
905 Ocean fronts and their influence on biological and physical processes in a changing
906 climate. *Nat. Clim. Change*, 10, 209–219. [https://doi.org/10.1038/s41558-020-0705-](https://doi.org/10.1038/s41558-020-0705-4)
907 [4](https://doi.org/10.1038/s41558-020-0705-4), 2020.

908 Clayson, C.A., Bogdanoff, A.S., 2013.: The Effect of Diurnal Sea Surface Temperature
909 Warming on Climatological Air–Sea Fluxes. *Am. Meteorol. Soc.*, 26, 2546–2556,
910 <https://doi.org/10.1175/JCLI-D-12-00062.1>, 2013.

911 Collins, M., An, S.-I., Cai, W., Ganachaud, A., Guilyardi, E., Jin, F.-F., Jochum, M., Lengaigne,
912 M., Power, S., Timmermann, A., Vecchi, G., Wittenberg, A., 2010.: The impact of
913 global warming on the tropical Pacific Ocean and El Niño. *Nat. Geosci.*, 3, 391–397,
914 <https://doi.org/10.1038/ngeo868>, 2010.

915 de Lavergne, C., Vic, C., Madec, G., Roquet, F., Waterhouse, A.F., Whalen, C.B., Cuyppers, Y.,
916 Bouruet-Aubertot, P., Ferron, B., Hibiya, T., 2020.: A Parameterization of Local and
917 Remote Tidal Mixing. *J. Adv. Model. Earth Syst.*, 12, e2020MS002065. <https://doi.org/10.1029/2020MS002065>,
918 <https://doi.org/10.1029/2020MS002065>, 2020.

919 de Macedo, C. R., Koch-Larrouy, A., da Silva, J. C. B., Magalhães, J. M., Lentini, C. A. D.,
920 Tran, T. K., Rosa, M. C. B., and Vantrepotte, V., 2023.: Spatial and temporal variability

921 [ofin](#) mode-1 and mode-2 internal solitary waves from MODIS/~~TERRA sun~~~~glint~~~~Terra~~
922 [sun glint](#) off the Amazon shelf (~~preprint~~). [Remote Sensing/Internal waves/Surface/Deep](#)
923 [Seas: Equatorial](#), [Ocean/Other. Sci.](#), 19, 1357–1374, [https://doi.org/10.5194/egusphere-](https://doi.org/10.5194/egusphere-2022-1482)
924 [2022-1482](#)os-19-1357-2023, 2023.

925 Didden, N., Schott, F., ~~1993~~.: Eddies in the North Brazil Current retroflection region observed
926 by Geosat altimetry. [J. Geophys. Res. Oceans](#), 98, 20121–20131, <https://doi.org/10.1029/93JC01184>, 1993.

927
928 Dong, S., Sprintall, J., Gille, S.T., Talley, L., ~~2008~~.: Southern Ocean mixed-layer depth from
929 Argo float profiles. [J. Geophys. Res. Oceans](#), 113, [C06013](#),
930 <https://doi.org/10.1029/2006JC004051>, 2008.

931 Dunphy, M., Lamb, K.G., ~~2014~~.: Focusing and vertical mode scattering of the first mode
932 internal tide by mesoscale eddy interaction. [J. Geophys. Res. Oceans](#), 119, 523–536,
933 <https://doi.org/10.1002/2013JC009293>, 2014.

934 Egbert, G.D., Ray, R.D., ~~2000~~.: Significant dissipation of tidal energy in the deep ocean
935 inferred from satellite altimeter data. [Nature](#), 405, 775–778,
936 <https://doi.org/10.1038/35015531>, 2000.

937 Fassoni-Andrade, A.C., Durand, F., Azevedo, A., Bertin, X., Santos, L.G., Khan, J.U., Testut,
938 L., Moreira, D.M., ~~2023~~.: Seasonal to interannual variability of the tide in the Amazon
939 estuary. [Cont. Shelf Res.](#), 255, 104945, <https://doi.org/10.1016/j.csr.2023.104945>,
940 [2023](#).

941 Fontes, R.F.C., Castro, B.M., Beardsley, R.C., ~~2008~~.: Numerical study of circulation on the
942 inner Amazon Shelf. [Ocean Dyn.](#), 58, 187–198, [https://doi.org/10.1007/s10236-008-](https://doi.org/10.1007/s10236-008-0139-4)
943 [0139-4](#), 2008.

944 Gabioux, M., Vinzon, S.B., Paiva, A.M., ~~2005~~.: Tidal propagation over fluid mud layers on the
945 Amazon shelf. [Cont. Shelf Res.](#), 25, 113–125,
946 <https://doi.org/10.1016/j.csr.2004.09.001>, 2005.

947 Garzoli, S.L., Ffield, A., Yao, Q., ~~2003~~.: North Brazil Current rings and the variability in the
948 latitude of retroflection, ~~in: Goni, G.J., Malanotte-Rizzoli, P. (Eds.), Elsevier~~
949 ~~Oceanography Series, [Interhemispheric Water Exchange in the Atlantic Ocean](#)~~
950 ~~Elsevier, pp.68~~, 357–373, [https://doi.org/10.1016/S0422-9894\(03\)80154-X](https://doi.org/10.1016/S0422-9894(03)80154-X), 2003.

951 Gévaudan, M., Durand, F., Jouanno, J., ~~2022~~.: Influence of the Amazon-Orinoco Discharge
952 Interannual Variability on the Western Tropical Atlantic Salinity and Temperature. [J.](#)
953 [Geophys. Res. Oceans](#), 127, [e2022JC018495](#), [JC018495](#),
954 <https://doi.org/10.1029/2022JC018495>, 2022.

955 Hernandez, O., Jouanno, J., Durand, F., ~~2016~~.: Do the Amazon and Orinoco freshwater plumes
956 really matter for hurricane-induced ocean surface cooling? [J. Geophys. Res. Oceans](#),
957 121, 2119–2141, <https://doi.org/10.1002/2015JC011021>, 2016.

958 Hernandez, O., Jouanno, J., Echevin, V., Aumont, O., ~~2017~~.: Modification of sea surface
959 temperature by chlorophyll concentration in the Atlantic upwelling systems. [J.](#)
960 [Geophys. Res. Oceans](#), 122, 5367–5389, <https://doi.org/10.1002/2016JC012330>,
961 [2017](#).

962 Hersbach, H., Bell, B., Berrisford, P., Hirahara, S., Horányi, A., Muñoz-Sabater, J., Nicolas, J.,
963 Peubey, C., Radu, R., Schepers, D., Simmons, A., Soci, C., Abdalla, S., Abellan, X.,
964 Balsamo, G., Bechtold, P., Biavati, G., Bidlot, J., Bonavita, M., De Chiara, G.,
965 Dahlgren, P., Dee, D., Diamantakis, M., Dragani, R., Flemming, J., Forbes, R., Fuentes,
966 M., Geer, A., Haimberger, L., Healy, S., Hogan, R.J., Hólm, E., Janisková, M., Keeley,
967 S., Laloyaux, P., Lopez, P., Lupu, C., Radnoti, G., de Rosnay, P., Rozum, I., Vamborg,
968 F., Villaume, S., Thépaut, J.-N., ~~2020~~.: The ERA5 global reanalysis. [Q. J. R. Meteorol.](#)
969 [Soc.](#), 146, 1999–2049, <https://doi.org/10.1002/qj.3803>, 2020.

970 Jayakrishnan, P.R., Babu, C.A., 2013.: Study of the Oceanic Heat Budget Components over
971 the Arabian Sea during the Formation and Evolution of Super Cyclone, Gonu 2013.,
972 Atmospheric and Climate Sciences, 3, 282-290,
973 <https://doi.org/10.4236/acs.2013.33030>, 2013.

974 Jithin, A.K., Francis, P.A., 2020.: Role of internal tide mixing in keeping the deep Andaman
975 Sea warmer than the Bay of Bengal. Sci. Rep., Scientific Reports, 10, 11982.,
976 <https://doi.org/10.1038/s41598-020-68708-6>, 2020.

977 ~~Johns, W.E., Lee, T.N., Schott, F.A., Zantopp, R.J., Evans, R.H.: The North Brazil Current~~
978 ~~retroflexion: Seasonal structure and eddy variability, J. Geophys. Res. Oceans, 95,~~
979 ~~22103-22120, <https://doi.org/10.1029/JC095iC12p22103>, 1990.~~

980 Johns, W.E., Lee, T.N., Beardsley, R.C., Candela, J., Limeburner, R., Castro, B., 1998.: Annual
981 Cycle and Variability of the North Brazil Current., J. Phys. Oceanogr., 28, 103–128.,
982 [https://doi.org/10.1175/1520-0485\(1998\)028<0103:ACAVOT>2.0.CO;2](https://doi.org/10.1175/1520-0485(1998)028<0103:ACAVOT>2.0.CO;2), 1998.

983 ~~Johns, W.E., Lee, T.N., Schott, F.A., Zantopp, R.J., Evans, R.H., 1990. The North Brazil~~
984 ~~Current retroflexion: Seasonal structure and eddy variability. J. Geophys. Res. Oceans~~
985 ~~95, 22103–22120. <https://doi.org/10.1029/JC095iC12p22103>~~

986 Jouanno, J., Marin, F., du Penhoat, Y., Sheinbaum, J., Molines, J.-M., 2011.: Seasonal heat
987 balance in the upper 100 m of the equatorial Atlantic Ocean., J. Geophys. Res. Oceans,
988 116., C09003, <https://doi.org/10.1029/2010JC006912>, 2011.

989 Kara, A.B., Rochford, P.A., Hurlburt, H.E., 2003.: Mixed layer depth variability over the
990 global ocean., J. Geophys. Res. Oceans, 108.(C3), 3079,
991 <https://doi.org/10.1029/2000JC000736>, 2003.

992 Kelly, S.M., Nash, J.D., Kunze, E., 2010.: Internal-tide energy over topography., J. Geophys.
993 Res. Oceans, 115., C06014, <https://doi.org/10.1029/2009JC005618>, 2010.

994 ~~Koch-Larrouy, A., Madec, G., Bouruet-Aubertot, P., Gerkema, T., Bessières, L., Molcard, R.:~~
995 ~~On the transformation of Pacific Water into Indonesian Throughflow Water by internal~~
996 ~~tidal mixing, Geophys. Res. Lett., 34, L04604, <https://doi.org/10.1029/2006GL028405>,~~
997 ~~2007.~~

998 ~~Koch-Larrouy, A., Madec, G., Iudicone, D., Atmadipoera, A., Molcard, R.: Physical processes~~
999 ~~contributing to the water mass transformation of the Indonesian Throughflow, Ocean~~
1000 ~~Dyn., 58, 275-288, <https://doi.org/10.1007/s10236-008-0154-5>, 2008.~~

1001 ~~Koch-Larrouy, A., Lengaigne, M., Terray, P., Madec, G., Masson, S.: Tidal mixing in the~~
1002 ~~Indonesian Seas and its effect on the tropical climate system, Clim. Dyn., 34, 891-904,~~
1003 ~~<https://doi.org/10.1007/s00382-009-0642-4>, 2010.~~

1004 Koch-Larrouy, A., Atmadipoera, A., van Beek, P., Madec, G., Aucan, J., Lyard, F., Grelet, J.,
1005 Souhaut, M., 2015.: Estimates of tidal mixing in the Indonesian archipelago from
1006 multidisciplinary INDOMIX in-situ data., Deep Sea Res. Part Oceanogr. Res. Pap.,
1007 106, 136–153., <https://doi.org/10.1016/j.dsr.2015.09.007>, 2015.

1008 ~~Koch-Larrouy, A., Lengaigne, M., Terray, P., Madec, G., Masson, S., 2010. Tidal mixing in the~~
1009 ~~Indonesian Seas and its effect on the tropical climate system. Clim. Dyn. 34, 891–904.~~
1010 ~~<https://doi.org/10.1007/s00382-009-0642-4>~~

1011 ~~Koch-Larrouy, A., Madec, G., Bouruet-Aubertot, P., Gerkema, T., Bessières, L., Molcard, R.,~~
1012 ~~2007. On the transformation of Pacific Water into Indonesian Throughflow Water by~~
1013 ~~internal tidal mixing. Geophys. Res. Lett. 34. <https://doi.org/10.1029/2006GL028405>~~

1014 ~~Koch-Larrouy, A., Madec, G., Iudicone, D., Atmadipoera, A., Molcard, R., 2008. Physical~~
1015 ~~processes contributing to the water mass transformation of the Indonesian Throughflow.~~
1016 ~~Ocean Dyn. 58, 275–288. <https://doi.org/10.1007/s10236-008-0154-5>~~

1017 Kosuth, P., Callède, J., Laraque, A., Filizola, N., Guyot, J.L., Seyler, P., Fritsch, J.M.,
1018 Guimarães, V., 2009.: Sea-tide effects on flows in the lower reaches of the Amazon
1019 River., Hydrol. Process., 23, 3141–3150., <https://doi.org/10.1002/hyp.7387>, 2009.

1020 Kunze, E., MacKay, C., McPhee-Shaw, E.E., Morrice, K., Girtton, J.B., Terker, S.R., 2012.:
1021 Turbulent Mixing and Exchange with Interior Waters on Sloping Boundaries. *J. Phys.*
1022 *Oceanogr.*, 42, 910–927. <https://doi.org/10.1175/JPO-D-11-075.1>, 2012.

1023 Lambeck, K., Runcorn, S.K., 1977.: Tidal dissipation in the oceans: astronomical, geophysical
1024 and oceanographic consequences. *Philos. Trans. R. Soc. Lond. Ser. Math. Phys. Sci.*,
1025 287, 545–594. <https://doi.org/10.1098/rsta.1977.0159>, 1977.

1026 Lascaratos, A., 1993.: Estimation of deep and intermediate water mass formation rates in the
1027 Mediterranean Sea. *Deep Sea Res. Part II Top. Stud. Oceanogr.*, 40, 1327–1332.
1028 [https://doi.org/10.1016/0967-0645\(93\)90072-U](https://doi.org/10.1016/0967-0645(93)90072-U), 1993.

1029 Laurent, L.S., Garrett, C., 2002.: The Role of Internal Tides in Mixing the Deep Ocean. *J.*
1030 *Phys. Oceanogr.*, 32, 2882–2899. [https://doi.org/10.1175/1520-0485\(2002\)032<2882:TROITI>2.0.CO;2](https://doi.org/10.1175/1520-0485(2002)032<2882:TROITI>2.0.CO;2), 2002.

1032 [Le Provost, C., Florent, L.: Energetics of the M2 barotropic ocean tides: an estimate of bottom
1033 friction dissipation from a hydrodynamic model, *Science Direct Prog. Oceanogr.*, 40\(1-
1034 4\), 37-52, \[https://doi.org/10.1016/S0079-6611\\(97\\)00022-0\]\(https://doi.org/10.1016/S0079-6611\(97\)00022-0\), 1997.](#)

1035 Leclair, M., Madec, G., 2009.: A conservative leapfrog time stepping method. *Ocean Model.*,
1036 30, 88–94. <https://doi.org/10.1016/j.ocemod.2009.06.006>, 2009.

1037 Lellouche, J.-M., Greiner, E., Le Galloudec, O., Garric, G., Regnier, C., Drevillon, M.,
1038 Benkiran, M., Testut, C.-E., Bourdalle-Badie, R., Gasparin, F., Hernandez, O., Levier,
1039 B., Drilllet, Y., Remy, E., Le Traon, P.-Y., 2018.: Recent updates to the Copernicus
1040 Marine Service global ocean monitoring and forecasting real-time 1/12° high-resolution
1041 system. *Ocean Sci.*, 14, 1093–1126. <https://doi.org/10.5194/os-14-1093-2018>, 2018.

1042 Lentini, C.A.D., Magalhães, J.M., da Silva, J.C.B., Lorenzetti, J.A., 2016.: Transcritical Flow
1043 and Generation of Internal Solitary Waves off the Amazon River: Synthetic Aperture
1044 Radar Observations and Interpretation. *Oceanography*, 29,(4), 187–195.
1045 <http://www.jstor.org/stable/24862294>, 2016.

1046 Lentz, S.J., Limeburner, R., 1995.: The Amazon River Plume during AMASSEDS: Spatial
1047 characteristics and salinity variability. *J. Geophys. Res. Oceans*, 100, 2355–2375.
1048 <https://doi.org/10.1029/94JC01411>, 1995.

1049 Li, C., Zhou, W., Jia, X., Wang, X., 2006.: Decadal/interdecadal variations of the ocean
1050 temperature and its impacts on climate. *Adv. Atmospheric Sci.*, 23, 964–981.
1051 <https://doi.org/10.1007/s00376-006-0964-7>, 2006.

1052 Li, Y., Curchitser, E.N., Wang, J., Peng, S., 2020.: Tidal Effects on the Surface Water Cooling
1053 Northeast of Hainan Island, South China Sea. *J. Geophys. Res. Oceans*, 125,
1054 [e2019JC016016.JC016016](https://doi.org/10.1029/2019JC016016), <https://doi.org/10.1029/2019JC016016>, 2020.

1055 Lyard, F.H., Allain, D.J., Cancet, M., Carrère, L., Picot, N., 2021.: FES2014 global ocean tide
1056 atlas: design and performance. *Ocean Sci.*, 17, 615–649. <https://doi.org/10.5194/os-17-615-2021>

1058 [Magalhaes, J.M., da Silva, J.C.B., Buijsman, M.C., Garcia, C. a. E., 2016. Effect of the North
1059 Equatorial Counter Current on the generation and propagation of internal solitary waves
1060 off the Amazon shelf \(SAR observations\). *Ocean Sci.*, 12, 243–255.
1061 <https://doi.org/10.5194/os-12-243-2016>](#)

1062 [Mei, W., Xie, S. P., Primeau, F., McWilliams, J.C., Pasquero, C., 2015. Northwestern Pacific
1063 typhoon intensity controlled by changes in ocean temperatures. *Sci. Adv.*, 1, e1500014.
1064 <https://doi.org/10.1126/sciadv.1500014>](#)

1065 [Moisan, J.R., Niiler, P.P., 1998. The Seasonal Heat Budget of the North Pacific: Net Heat Flux
1066 and Heat Storage Rates \(1950–1990\). *J. Phys. Oceanogr.*, 28, 401–421.
1067 \[https://doi.org/10.1175/1520-0485\\(1998\\)028<0401:TSHBOT>2.0.CO;2\]\(https://doi.org/10.1175/1520-0485\(1998\)028<0401:TSHBOT>2.0.CO;2\)](#)

1068 [Muller-Karger, F.E., McClain, C.R., Richardson, P.L., 1988. The dispersal of the Amazon's
1069 water. *Nature* 333, 56–59. <https://doi.org/10.1038/333056a0>](#)

1070 [Munk, W., Wunsch, C., 1998. Abyssal recipes II: energetics of tidal and wind mixing. Deep](#)
1071 [Sea Res. Part Oceanogr. Res. Pap. 45, 1977-2010. \[https://doi.org/10.1016/S0967-\]\(https://doi.org/10.1016/S0967-0637\(98\)00070-3\)](#)
1072 [0637\(98\)00070-3](#)

1073 [Nagai, T., Hibiya, T., 2015. Internal tides and associated vertical mixing in the Indonesian](#)
1074 [Archipelago. J. Geophys. Res. Oceans 120, 3373-3390.](#)
1075 <https://doi.org/10.1002/2014JC010592>, 2021.

1076 [Madec, G., Bourdallé-Badie, R., Chanut, J., Clementi, E., Coward, A., Ethé, C., Iovino, D., Lea,](#)
1077 [D., Lévy, C., Lovato, T., Martin, N., Masson, S., Mocavero, S., Rousset, C., Storkey,](#)
1078 [D., Vancoppenolle, M., Müeller, S., Nurser, G., Bell, M., & Samson, G., 2019. NEMO](#)
1079 [ocean engine. In Notes du Pôle de modélisation de l'Institut Pierre-Simon Laplace](#)
1080 [\(IPSL\) \(v4.0, Numéro 27\). Zenodo. \[10.5281\],](#)
1081 <https://doi.org/10.5281/zenodo.3878122>, 2019.

1082 [Magalhaes, J.M., da Silva, J.C.B., Buijsman, M.C., Garcia, C. a. E.: Effect of the North](#)
1083 [Equatorial Counter Current on the generation and propagation of internal solitary waves](#)
1084 [off the Amazon shelf \(SAR observations\), Ocean Sci., 12, 243-255,](#)
1085 <https://doi.org/10.5194/os-12-243-2016>, 2016.

1086 [Mei, W., Xie, S.-P., Primeau, F., McWilliams, J.C., Pasquero, C.: Northwestern Pacific typhoon](#)
1087 [intensity controlled by changes in ocean temperatures, Sci. Adv., 1, e1500014,](#)
1088 <https://doi.org/10.1126/sciadv.1500014>, 2015.

1089 [Moisan, J.R., Niiler, P.P.: The Seasonal Heat Budget of the North Pacific: Net Heat Flux and](#)
1090 [Heat Storage Rates \(1950–1990\), J. Phys. Oceanogr., 28, 401-421,](#)
1091 [https://doi.org/10.1175/1520-0485\(1998\)028<0401:TSHBOT>2.0.CO;2](https://doi.org/10.1175/1520-0485(1998)028<0401:TSHBOT>2.0.CO;2), 1998.

1092 [Muller-Karger, F.E., McClain, C.R., Richardson, P.L.: The dispersal of the Amazon's water,](#)
1093 [Nature, 333, 56-59, <https://doi.org/10.1038/333056a0>, 1988.](#)

1094 [Munk, W., Wunsch, C.: Abyssal recipes II: energetics of tidal and wind mixing, Deep Sea Res.](#)
1095 [Part Oceanogr. Res. Pap., 45, 1977-2010, \[https://doi.org/10.1016/S0967-\]\(https://doi.org/10.1016/S0967-0637\(98\)00070-3\)](#)
1096 [0637\(98\)00070-3](#), 1998.

1097 [Nagai, T., Hibiya, T.: Internal tides and associated vertical mixing in the Indonesian](#)
1098 [Archipelago, J. Geophys. Res. Oceans, 120, 3373-3390,](#)
1099 <https://doi.org/10.1002/2014JC010592>, 2015.

1100 [Neto, A.V.N., da Silva, A.C., 2014. Seawater temperature changes associated with the North](#)
1101 [Brazil current dynamics. Ocean Dyn., 64, 13–27, \[https://doi.org/10.1007/s10236-\]\(https://doi.org/10.1007/s10236-013-0667-4\)](#)
1102 [013-0667-4](#), 2014.

1103 [Niwa, Y., Hibiya, T., 2011. Estimation of baroclinic tide energy available for deep ocean](#)
1104 [mixing based on three-dimensional global numerical simulations. J. Oceanogr., 67,](#)
1105 [493–502, <https://doi.org/10.1007/s10872-011-0052-1>, 2011.](#)

1106 [Nugroho, D., Koch-Larrouy, A., Gaspar, P., Lyard, F., Reffray, G., Tranchant, B., 2018. Modelling explicit tides in the Indonesian sea: An important process for surface sea water properties. Mar. Pollut. Bull. Special Issue: Indonesia seas management, 131, 7–18, <https://doi.org/10.1016/j.marpolbul.2017.06.033>, 2018.](#)

1110 [Peng, S., Liao, J., Wang, X., Liu, Z., Liu, Y., Zhu, Y., Li, B., Khokiattiwong, S., Yu, W., 2021. Energetics Based Estimation of the Diapycnal Mixing Induced by Internal Tides in the Andaman Sea. J. Geophys. Res. Oceans, 126, e2020JC016521, <https://doi.org/10.1029/2020JC016521>, 2021.](#)

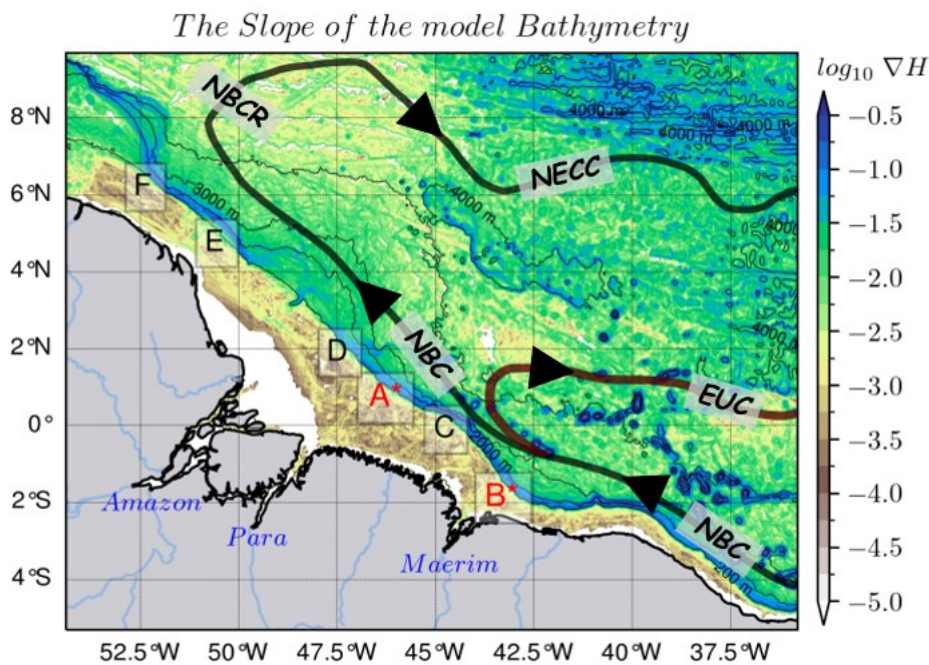
1114 [Prestes, Y.O., Silva, A.C. da, Jeandel, C., 2018. Amazon water lenses and the influence of the North Brazil Current on the continental shelf. Cont. Shelf Res., 160, 36–48. <https://doi.org/10.1016/j.csr.2018.04.002>, 2018.](#)

1117 [Richardson, P.L., Hufford, G.E., Limeburner, R., Brown, W.S., 1994. North Brazil Current retroflection eddies. J. Geophys. Res. Oceans, 99, 5081–5093. <https://doi.org/10.1029/93JC03486>, 1994.](#)

- 1120 Rosenthal, Y., Boyle, E.A., Slowey, N., 1997.: Temperature control on the incorporation of
1121 magnesium, strontium, fluorine, and cadmium into benthic foraminiferal shells from
1122 Little Bahama Bank: Prospects for thermocline paleoceanography. *Geochim.*
1123 *Cosmochim. Acta.* 61, 3633–3643. [https://doi.org/10.1016/S0016-7037\(97\)00181-6](https://doi.org/10.1016/S0016-7037(97)00181-6),
1124 [1997](https://doi.org/10.1016/S0016-7037(97)00181-6).
- 1125 Ruault, V., Jouanno, J., Durand, F., Chanut, J., Benshila, R., 2020.: Role of the Tide on the
1126 Structure of the Amazon Plume: A Numerical Modeling Approach. *J. Geophys. Res.*
1127 *Oceans*, 125, e2019JC015495. <https://doi.org/10.1029/2019JC015495>, 2020.
- 1128 Salamena, G.G., Whinney, J.C., Heron, S.F., Ridd, P.V., 2021.: Internal tidal waves and deep-
1129 water renewal in a tropical fjord: Lessons from Ambon Bay, eastern Indonesia. *Estuar.*
1130 *Coast. Shelf Sci.*, 253, 107291. <https://doi.org/10.1016/j.ecss.2021.107291>, 2021.
- 1131 Schott, F.A., Dengler, M., Brandt, P., Affler, K., Fischer, J., Bourlès, B., Gouriou, Y., Molinari,
1132 R.L., Rhein, M., 2003.: The zonal currents and transports at 35°W in the tropical
1133 Atlantic. *Geophys. Res. Lett.*, 30(7), 1349, <https://doi.org/10.1029/2002GL016849>,
1134 [2003](https://doi.org/10.1029/2002GL016849).
- 1135 ~~Sharples, J., Moore, C.M., Hickman, A.E., Holligan, P.M., Tweddle, J.F., Palmer, M.R.,~~
1136 ~~Simpson, J.H., 2009. Internal tidal mixing as a control on continental margin~~
1137 ~~ecosystems. *Geophys. Res. Lett.* 36. <https://doi.org/10.1029/2009GL040683>~~
- 1138 Sharples, J., Tweddle, J.F., Green, J.A.M., Palmer, M.R., Kim, Y.-N., Hickman, A.E., Holligan,
1139 P.M., Moore, C.M., Rippeth, T.P., Simpson, J.H., Krivtsov, V., 2007.: Spring-neap
1140 modulation of internal tide mixing and vertical nitrate fluxes at a shelf edge in summer.
1141 *Limnol. Oceanogr.*, 52, 1735–1747. <https://doi.org/10.4319/lo.2007.52.5.1735>, 2007.
- 1142 ~~Sharples, J., Moore, C.M., Hickman, A.E., Holligan, P.M., Tweddle, J.F., Palmer, M.R.,~~
1143 ~~Simpson, J.H.: Internal tidal mixing as a control on continental margin ecosystems,~~
1144 ~~*Geophys. Res. Lett.*, 36, L23603, <https://doi.org/10.1029/2009GL040683>, 2009.~~
- 1145 Silva, A., Araujo, M., Medeiros, C., Silva, M., Bourles, B., 2005.: Seasonal changes in the
1146 mixed and barrier layers in the western Equatorial Atlantic. *Braz. J. Oceanogr.*, 53(3-
1147 4), 83–98, <https://doi.org/10.1590/S1679-87592005000200001>, 2005.
- 1148 Smith, J.E., Smith, C.M., Vroom, P.S., Beach, K.L., Miller, S., 2004.: Nutrient and growth
1149 dynamics of Halimeda tuna on Conch Reef, Florida Keys: Possible influence of internal
1150 tides on nutrient status and physiology. *Limnol. Oceanogr.*, 49, 1923–1936.
1151 <https://doi.org/10.4319/lo.2004.49.6.1923>, 2004.
- 1152 Smith, K.A., Rocheleau, G., Merrifield, M.A., Jaramillo, S., Pawlak, G., 2016.: Temperature
1153 variability caused by internal tides in the coral reef ecosystem of Hanauma bay,
1154 Hawai‘i. *Cont. Shelf Res.*, 116, 1–12. <https://doi.org/10.1016/j.csr.2016.01.004>,
1155 [2016](https://doi.org/10.1016/j.csr.2016.01.004).
- 1156 Speer, K.G., Isemer, H.-J., Biastoch, A., 1995.: Water mass formation from revised COADS
1157 data. *J. Phys. Oceanogr.*, 25(10), 2444–2457, [https://doi.org/10.1175/1520-0485\(1995\)025<2444:WMFFRC>2.0.CO;2](https://doi.org/10.1175/1520-0485(1995)025<2444:WMFFRC>2.0.CO;2), 1995.
- 1159 Sprintall, J., Gordon, A.L., Koch-Larrouy, A., Lee, T., Potemra, J.T., Pujiana, K., Wijffels, S.E.,
1160 2014.: The Indonesian seas and their role in the coupled ocean–climate system. *Nat.*
1161 *Geosci.*, 7, 487–492. <https://doi.org/10.1038/ngeo2188>, 2014.
- 1162 Sprintall, J., Gordon, A.L., Wijffels, S.E., Feng, M., Hu, S., Koch-Larrouy, A., Phillips, H.,
1163 Nugroho, D., Napitu, A., Pujiana, K., Susanto, R.D., Sloyan, B., Peña-Molino, B., Yuan,
1164 D., Riama, N.F., Siswanto, S., Kuswardani, A., Arifin, Z., Wahyudi, A.J., Zhou, H.,
1165 Nagai, T., Ansong, J.K., Bourdalle-Badié, R., Chanut, J., Lyard, F., Arbic, B.K.,
1166 Ramdhani, A., Setiawan, A., 2019.: Detecting Change in the Indonesian Seas. *Front.*
1167 *Mar. Sci.*, 6, 257, <https://doi.org/10.3389/fmars.2019.00257>, 2019.

- 1168 Swift, J.H., Aagaard, K., ~~1981.~~: Seasonal transitions and water mass formation in the Iceland
1169 and Greenland seas. *Deep Sea Res. Part Oceanogr. Res. Pap.*, 28, 1107–1129.
1170 [https://doi.org/10.1016/0198-0149\(81\)90050-9](https://doi.org/10.1016/0198-0149(81)90050-9), 1981.
- 1171 ~~Tchilibou, M., Gourdeau, L., Lyard, F., Morrow, R., Koch-Larrouy, A., Allain, D., Djath, B.,
1172 2020. Internal tides in the Solomon Sea in contrasted ENSO conditions. *Ocean Sci.* 16,
1173 615–635. <https://doi.org/10.5194/os-16-615-2020>~~
- 1174 Tchilibou, M., Gourdeau, L., Morrow, R., Serazin, G., Djath, B., Lyard, F., ~~2018.~~: Spectral
1175 signatures of the tropical Pacific dynamics from model and altimetry: a focus on the
1176 meso-/submesoscale range. *Ocean Sci.*, 14, 1283–1301. [https://doi.org/10.5194/os-](https://doi.org/10.5194/os-14-1283-2018)
1177 [14-1283-2018](https://doi.org/10.5194/os-14-1283-2018), 2018.
- 1178 ~~Tchilibou, M., Gourdeau, L., Lyard, F., Morrow, R., Koch-Larrouy, A., Allain, D., Djath, B.:
1179 Internal tides in the Solomon Sea in contrasted ENSO conditions, *Ocean Sci.*, 16, 615-
1180 635, <https://doi.org/10.5194/os-16-615-2020>, 2020.~~
- 1181 Tchilibou, M., Koch-Larrouy, A., Barbot, S., Lyard, F., Morel, Y., Jouanno, J., Morrow, R.,
1182 ~~2022.~~: Internal tides off the Amazon shelf during two contrasted seasons: interactions
1183 with background circulation and SSH imprints. *Ocean Sci.*, 18, 1591–1618.
1184 <https://doi.org/10.5194/os-18-1591-2022>, 2022.
- 1185 Varona, H.L., Veleda, D., Silva, M., Cintra, M., Araujo, M., ~~2019.~~: Amazon River plume
1186 influence on Western Tropical Atlantic dynamic variability. *Dyn. Atmospheres
1187 Oceans*, 85, 1–15. <https://doi.org/10.1016/j.dynatmoce.2018.10.002>, 2019.
- 1188 Vlasenko, V., Stashchuk, N., ~~2006.~~: Amplification and Suppression of Internal Waves by Tides
1189 over Variable Bottom Topography. *J. Phys. Oceanogr.*, 36, 1959–1973.
1190 <https://doi.org/10.1175/JPO2958.1>, 2006.
- 1191 Wang, X., Peng, S., Liu, Z., Huang, R.X., Qian, Y.-K., Li, Y., ~~2016.~~: Tidal Mixing in the South
1192 China Sea: An Estimate Based on the Internal Tide Energetics. *J. Phys. Oceanogr.*, 46,
1193 107–124. <https://doi.org/10.1175/JPO-D-15-0082.1>, 2016.
- 1194 Wentz, F.J., ~~2015.~~: A 17-Yr Climate Record of Environmental Parameters Derived from the
1195 Tropical Rainfall Measuring Mission (TRMM) Microwave Imager. *J. Clim., Journal of
1196 Climate*, 28, 6882–6902. <https://doi.org/10.1175/JCLI-D-15-0155.1>, 2015.
- 1197 Whalen, C.B., Talley, L.D., MacKinnon, J.A., ~~2012.~~: Spatial and temporal variability of global
1198 ocean mixing inferred from Argo profiles. *Geophys. Res. Lett.*, 39, L18612,
1199 <https://doi.org/10.1029/2012GL053196>, 2012.
- 1200 Xie, S.-P., Carton, J.A., ~~2004.~~: Tropical Atlantic variability: Patterns, mechanisms, and
1201 impacts. *Wash. DC Am. Geophys. Union Geophys. Monogr. Ser.*, 147, 121–142.
1202 <https://doi.org/10.1029/147GM07>, 2004.
- 1203 Xu, P., Yang, W., Zhu, B., Wei, H., Zhao, L., Nie, H., ~~2020.~~: Turbulent mixing and vertical
1204 nitrate flux induced by the semidiurnal internal tides in the southern Yellow Sea. *Cont.
1205 Shelf Res.*, 208, 104240. <https://doi.org/10.1016/j.csr.2020.104240>, 2020.
- 1206 Yadidya, B., Rao, A.D., ~~2022.~~: Projected climate variability of internal waves in the Andaman
1207 Sea. *Commun. Earth Environ.*, 3, 1–12. [https://doi.org/10.1038/s43247-022-00574-](https://doi.org/10.1038/s43247-022-00574-8)
1208 [8](https://doi.org/10.1038/s43247-022-00574-8), 2022.
- 1209 Zalesak, S.T., ~~1979.~~ Fully multidimensional flux-corrected transport algorithms for fluids. *J.
1210 Comput. Phys.*, 31, 335–362. [https://doi.org/10.1016/0021-9991\(79\)90051-2](https://doi.org/10.1016/0021-9991(79)90051-2), 1979.
- 1211 Zaron, E.D., ~~2019.~~: Baroclinic Tidal Sea Level from Exact-Repeat Mission Altimetry. *J. Phys.
1212 Oceanogr.*, 49, 193–210. <https://doi.org/10.1175/JPO-D-18-0127.1>, 2019.

1216
 1217
 1218
 1219
 1220
 1221
 1222
 1223
 1224
 1225
 1226
 1227
 1228



1229
 1230
 1231
 1232
 1233
 1234
 1235
 1236
 1237
 1238
 1239

Figure 1. The horizontal gradient (∇H) of the model's bathymetry (∇H) with ~~different~~ internal tides generation sites (A*, B*, C, D, E and F) along the high slope of the shelf break (blue color shading) ~~of the shelf break~~, with the two main sites A* and B* (in red), as reported in Magalhaes et al. (2016) and Tchilibou et al. (2022). Solid bold lines represent a schematic view of the circulation (as described by Didden and Schott, 1993; Richardson et al., 1994; Johns et al., 1998; Bourles et al., 1999a; Schott et al., 2003; Garzoli et al., 2004) with NBC, NBCR and NECC tracks in black, and the EUC track in brown red. Tin black contours are 200 m, 2000 m, 3000 m and 4000 m isobaths from the model bathymetry.

1240

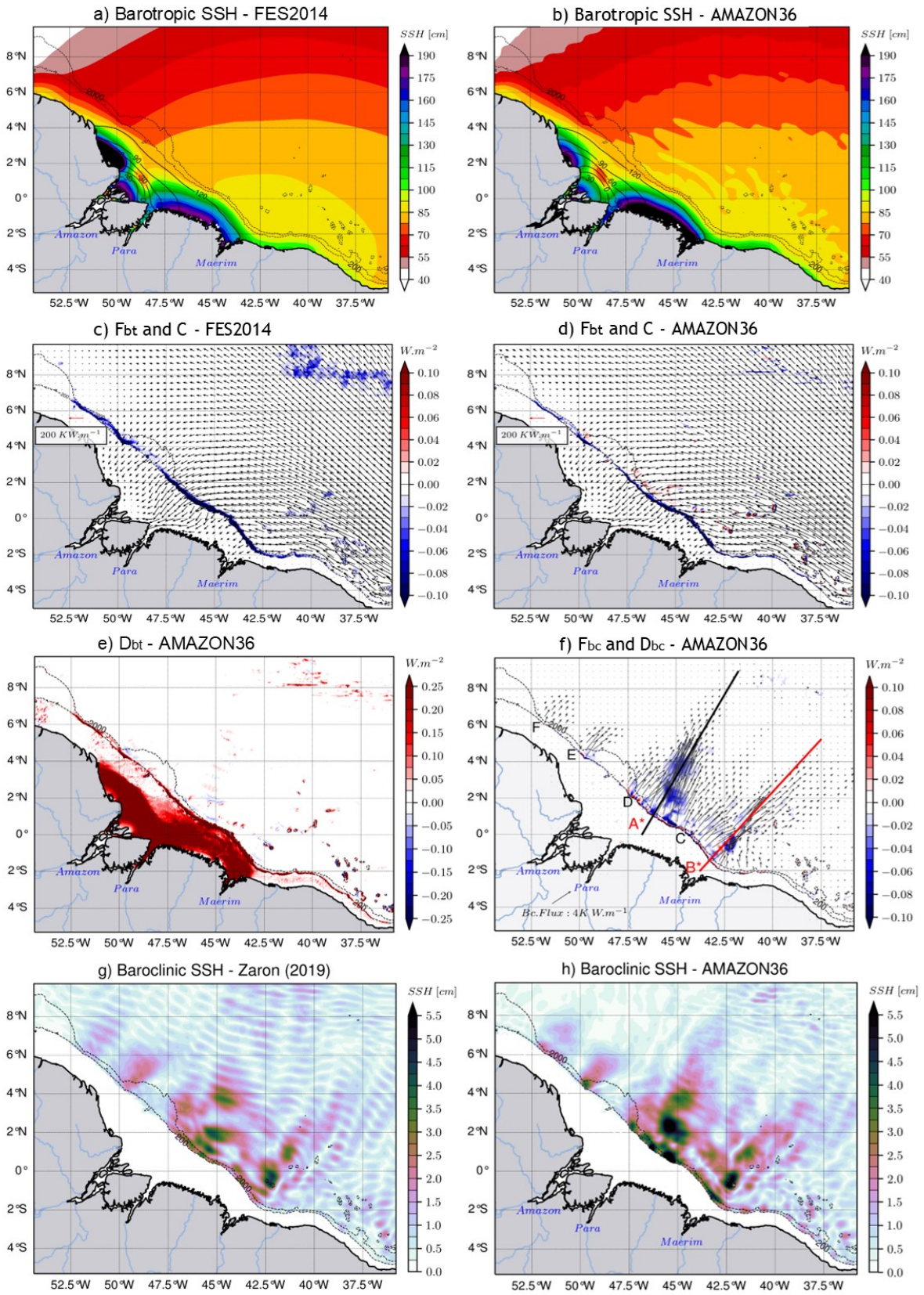
1241

1242

1243

1244

1245



bt : barotropic ; bc : baroclinic
 F : energy flux ; C : barotropic-to-baroclinic energy conversion ; D : dissipation

1246
 1247

Figure 2. *Coherent (or stationary) characteristics* Characteristics of the M_2 coherent tides.

1248 *Barotropic sea surface height (color shading) and its phase (solid contours) for (a) FES2014*
1249 *and (b) the model, barotropic energy flux (black arrows) with the energy conversion rate (color*
1250 *shading) for (c) FES2014 and (d) the model, (e) the model depth-integrated barotropic energy*
1251 *dissipation, (f) the model depth-integrated baroclinic energy flux (black arrows) and the depth-*
1252 *integrated baroclinic energy dissipation (color shading) with transect lines along IT*
1253 *trajectories A* (black) and B* (red), the baroclinic sea surface height from (g) Zaron (2019)*
1254 *and (h) the model. Data from the model are the mean value over the year 2015. For all panels,*
1255 *dashed black ~~lines~~ contours represent the 200 m and 2000 m isobaths of the model bathymetry.*

1256

1257

1258

1259

1260

1261

1262

1263

1264

1265

1266

1267

1268

1269

1270

1271

1272

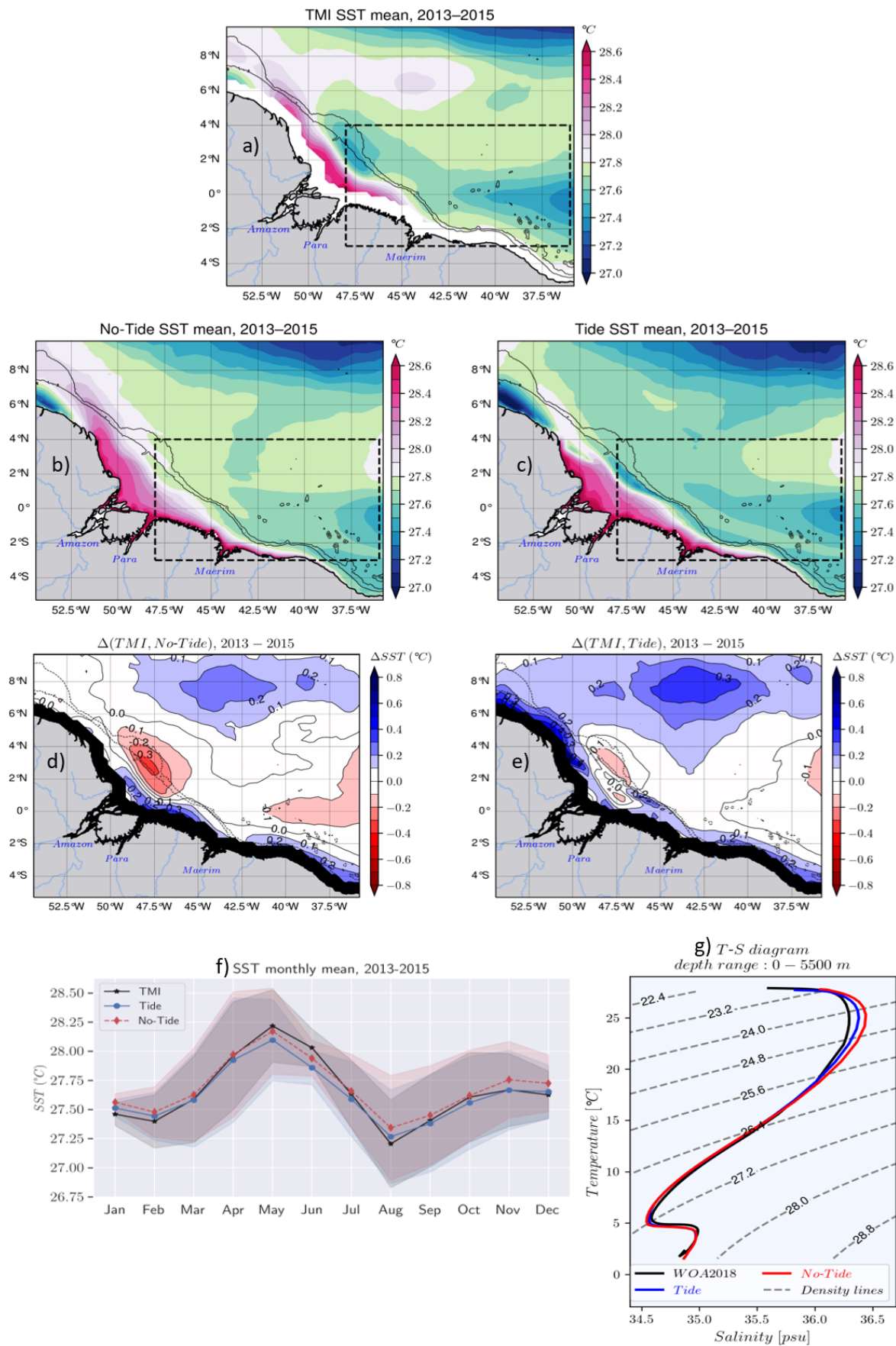
1273

1274

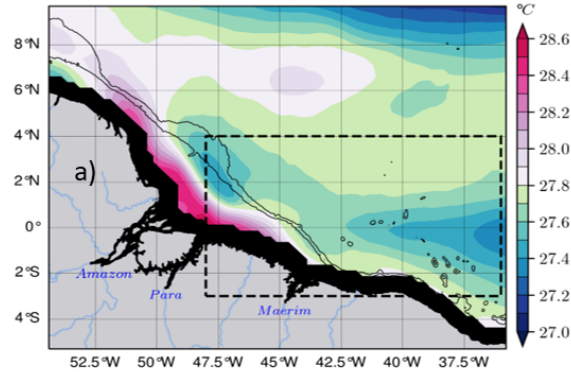
1275

1276

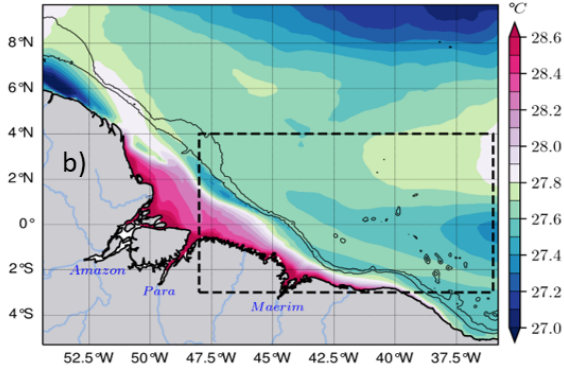
1277



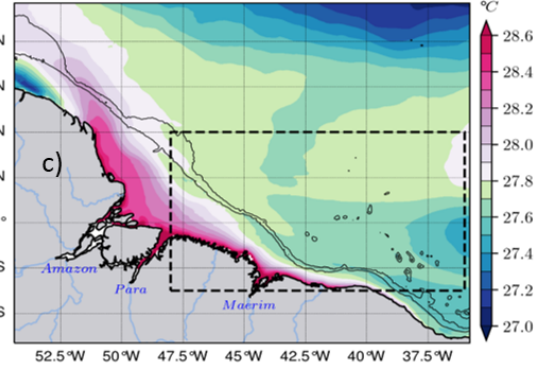
TMI SST mean, 2013–2015



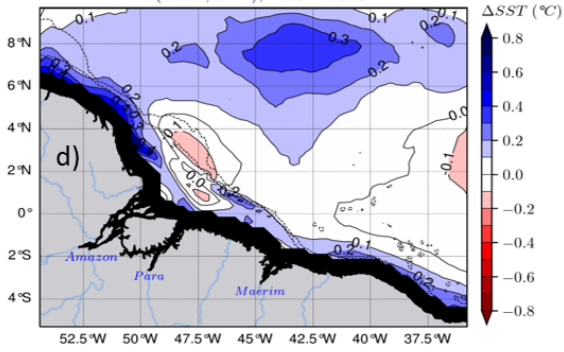
Tide SST mean, 2013–2015



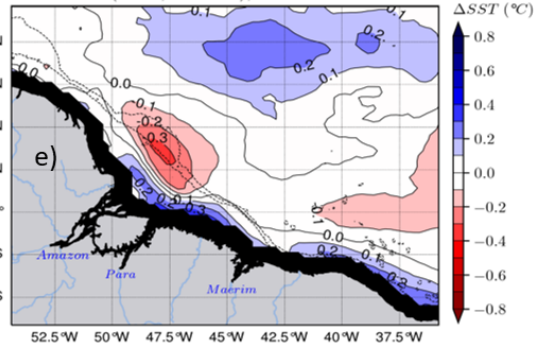
No-Tide SST mean, 2013–2015



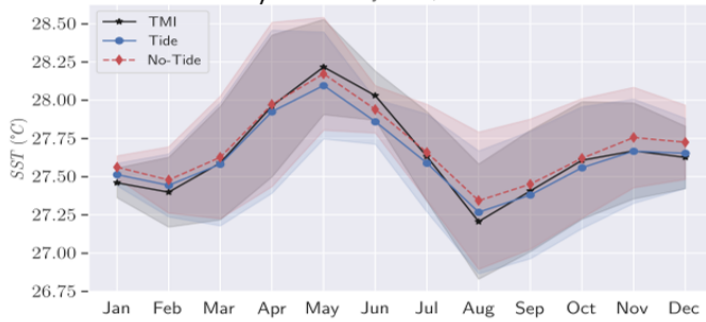
$\Delta(TMI, Tide)$, 2013 – 2015



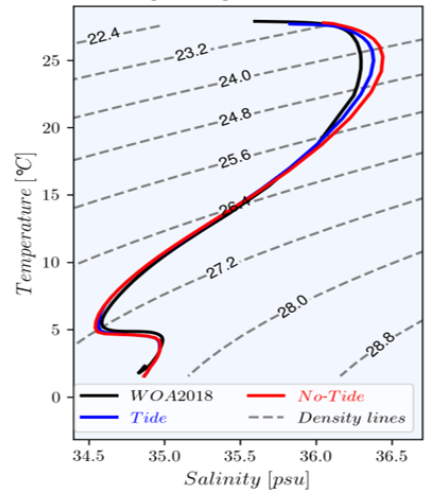
$\Delta(TMI, No-Tide)$, 2013 – 2015



f) SST monthly mean, 2013–2015

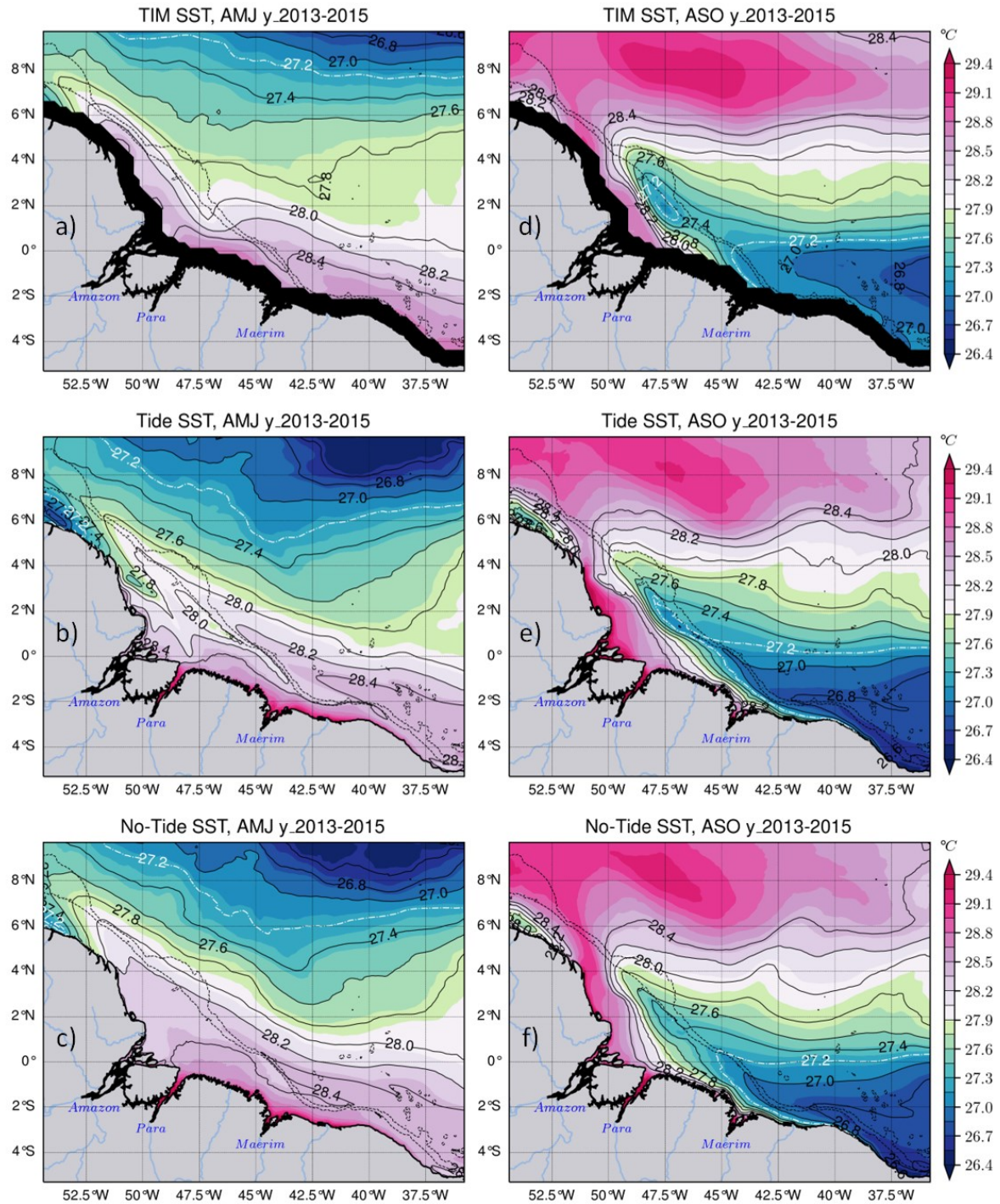


g) T-S diagram
depth range : 0 – 5500 m



1281 *Figure 3. Validation of the model temperature for the whole period 2013-2015. Mean SST for*
1282 *(a) TMI with its black coastal mask, (b) the -tidal simulation, (c) the -non-tidal simulation, the*
1283 *difference (bias) in SST between TMI and (d) the tidal ~~simulations~~simulations and (e) the non-*
1284 *tidal simulation, (f) the seasonal cycle of the SST of the three products averaged within the*
1285 *dashed ~~line~~-box in upper panels covering IT pathways with values masked below the 200 m*
1286 *isobath, bands indicate variability according to standard deviation. Solid black lines in panels*
1287 *a--c and dashed black lines in panels d--e represent the 200 m and 2000 m isobaths from the*
1288 *model bathymetry, while solid black lines in panels d--e represent bias contours. (g)*
1289 *Temperature-Salinity (T-S) diagram of the mean properties in the same area as (f) from*
1290 *observed WOA2018 climatology (black line), the tidal ~~simulations~~simulations (blue line) and*
1291 *non-tidal ~~simulations~~simulations (red line) for the water column from surface to 5500 m depth,*
1292 *dashed gray lines represent density (σ_θ) contours.*

1293
1294
1295
1296
1297
1298
1299
1300
1301
1302
1303
1304
1305
1306
1307
1308
1309
1310
1311
1312
1313
1314
1315
1316
1317



1318

1319

1320

1321

1322

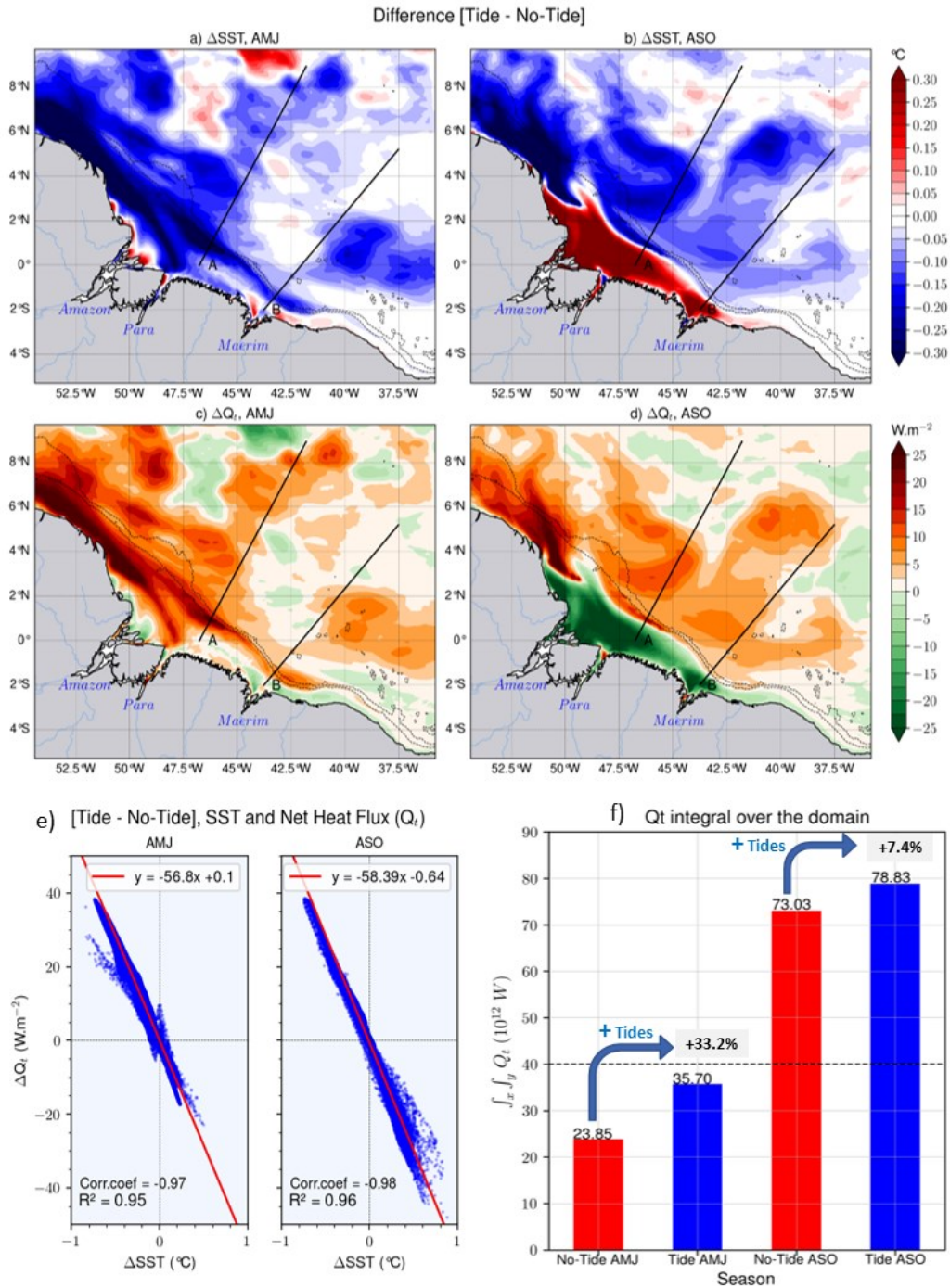
1323

1324

1325

1326

Figure 4. 2013-2015 seasonal SST mean. The left panels stand for the AMJ season for TMI with its black coastal mask, the tidal ~~simulations~~ and the non-tidal ~~simulations~~, respectively for the upper-left, center-left and lower-left panel; the same in the panels on the right but for ~~the~~ ASO season. The dashed white and black solid lines represent the temperature contours. Dashed black lines in all panels stand for the 200 m and 2000 m isobaths from the model bathymetry.



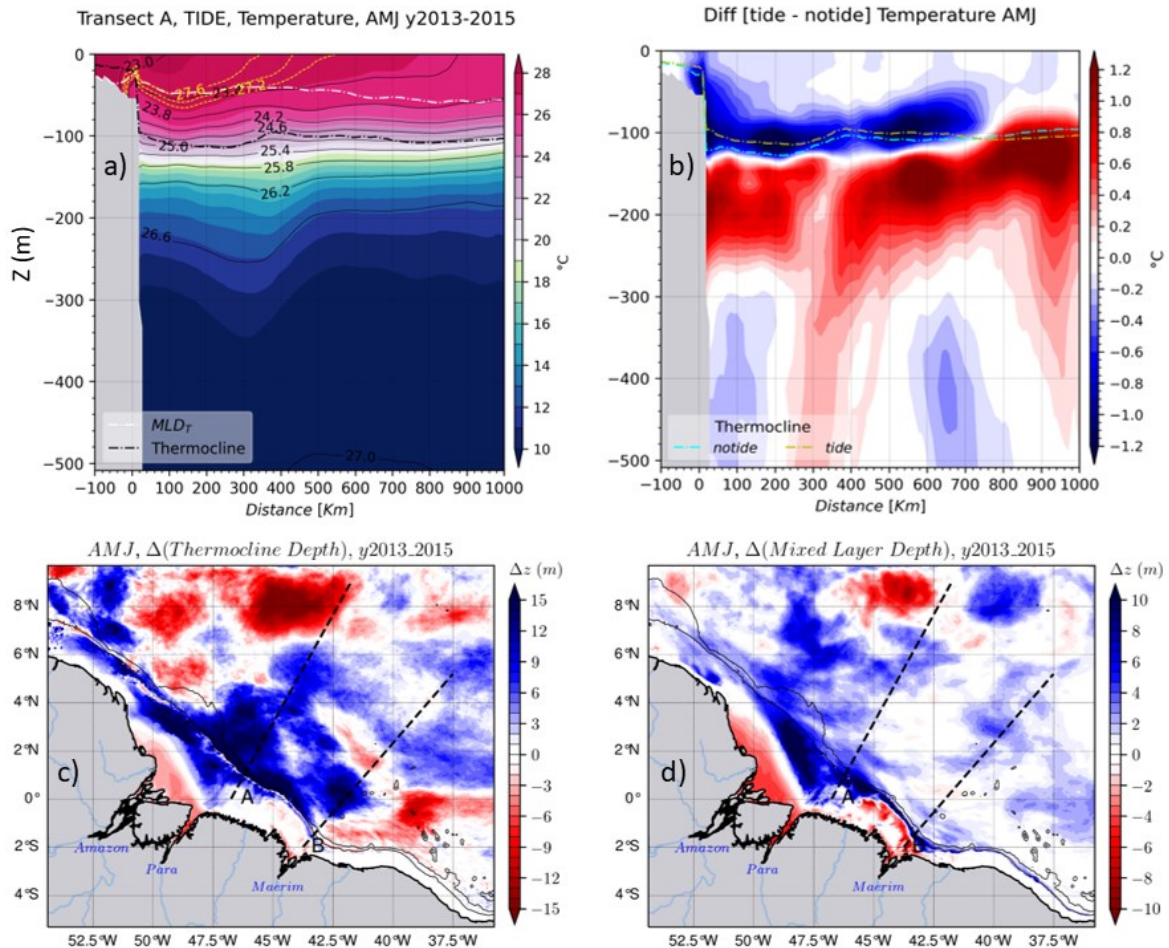
1327

1328 *Figure 5. Relationship between the SST and the atmosphere-to-ocean net heat flux (Q_t): SST*
 1329 *anomaly [Tide - No-Tide] in AMJ (a) and ASO (b) seasons, Q_t anomaly in AMJ (c) and ASO*
 1330 *seasons, (e) correlation between Q_t anomaly and SST anomaly for each season, (f) domain*
 1331 *integrated Q_t for both seasons of each simulation. Dashed black lines in panels a-d stand for*
 1332 *the 200 m and 2000 m isobaths from the model bathymetry.*
 1333

1334

1335

1336



1337

1338

1339

1340

1341

1342

1343

1344

1345

1346

1347

1348

1349

1350

1351

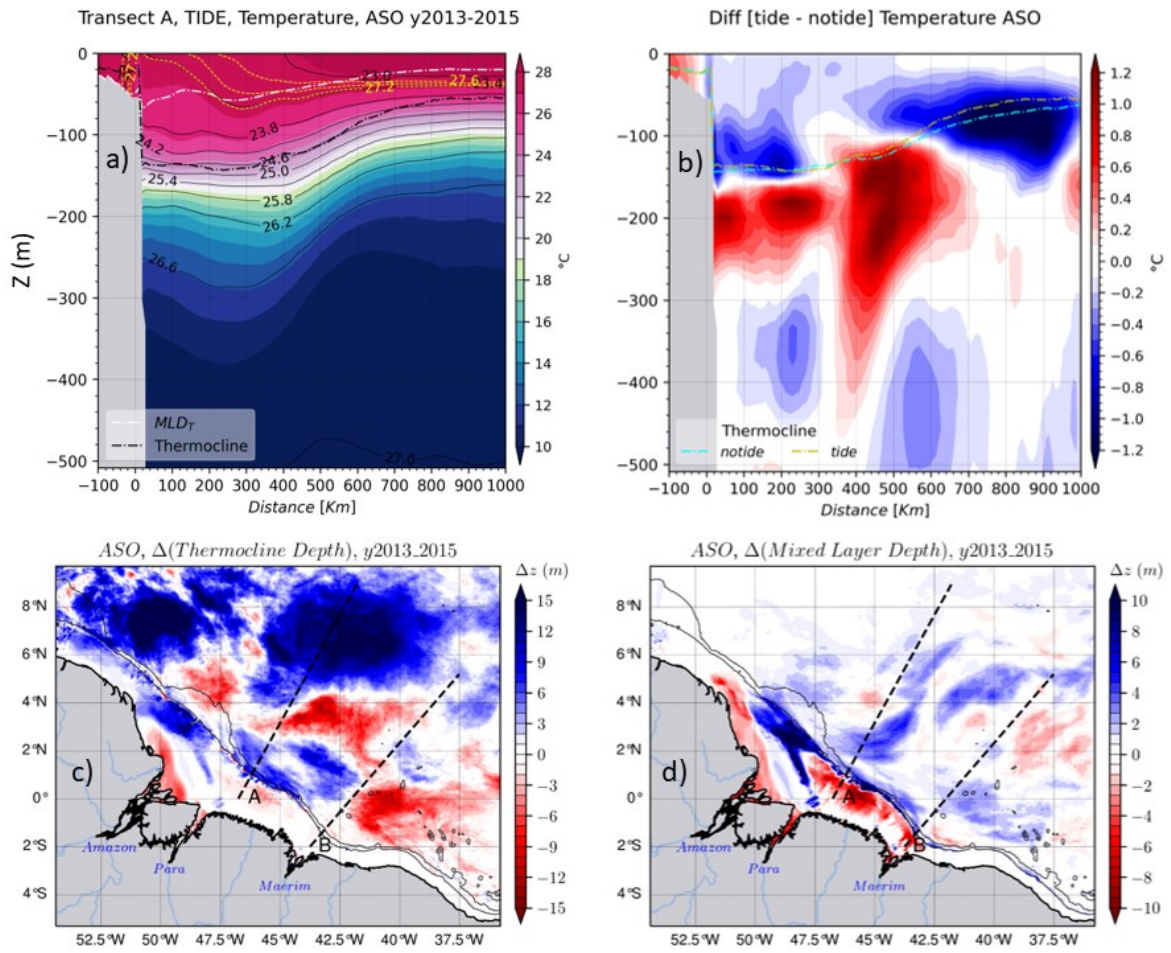
1352

1353

1354

1355

Figure 6. ~~Some water~~Water mass properties for the AMJ season: (a) vertical section of the temperature of the tidal ~~simulations~~simulations following the transect A, -the yellow dashed and the solid black lines are the temperature and density (σ_{θ}) contours, respectively, -the. The black and white ticked dashed lines are the thermocline and MLD_r , respectively. (b) the temperature anomaly for the same vertical section, yellow and cyan dashed lines are the thermocline depth for the tidal and non-tidal simulations, respectively. (c) thermocline depth anomaly and (d) MLD anomaly for the whole domain. ~~When~~The blue (vs red) color shading in the MLD or the Thermocline depth anomaly ~~are colored in blue (vs red) it means that~~the tides rise (vs deepen) them. Solid black lines in lower panels stand for the 200 m and 2000 m isobaths from the model bathymetry.



1357

1358

Figure 7. Same as figure 6 but for the ASO season.

1359

1360

1361

1362

1363

1364

1365

1366

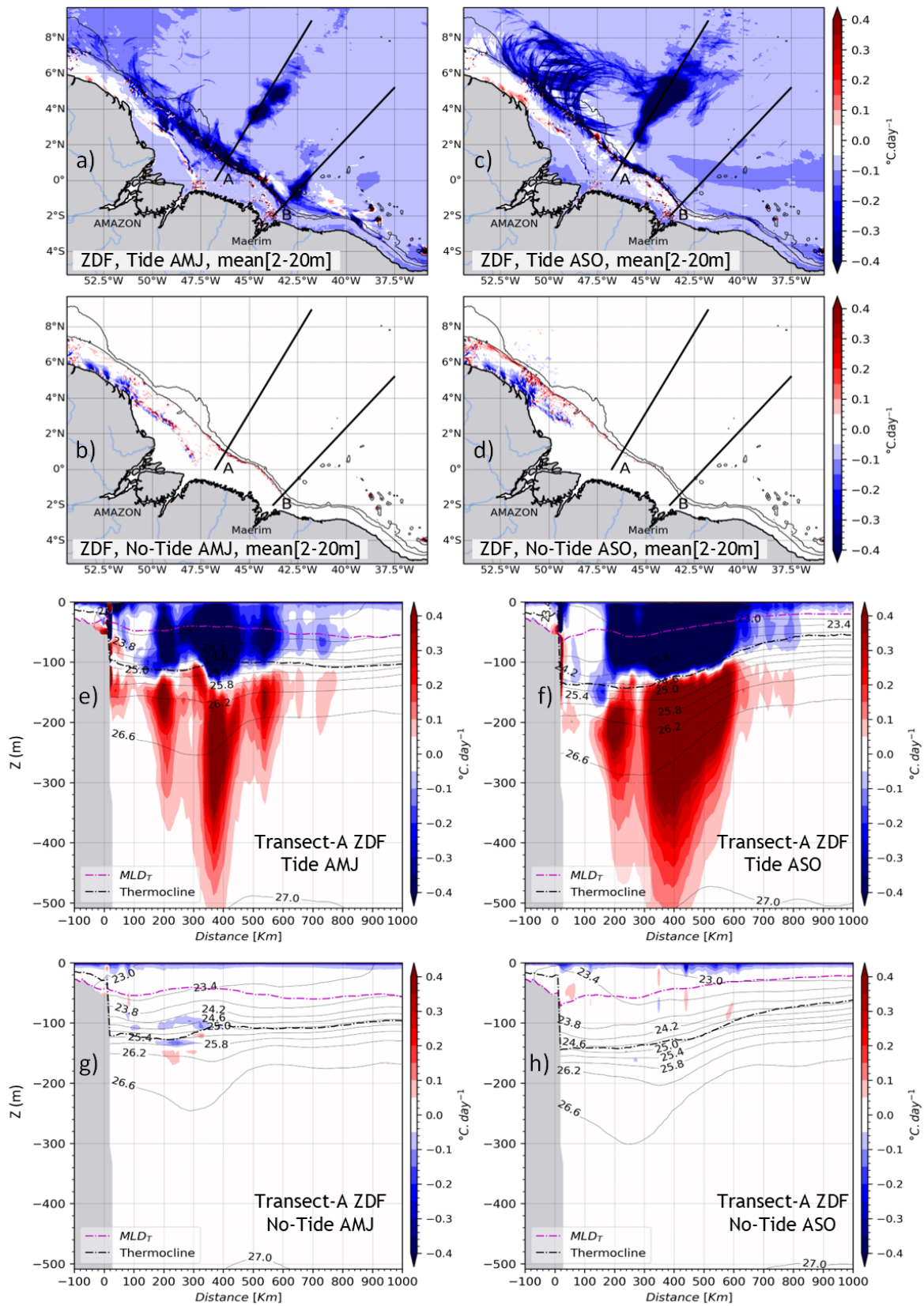
1367

1368

1369

1370

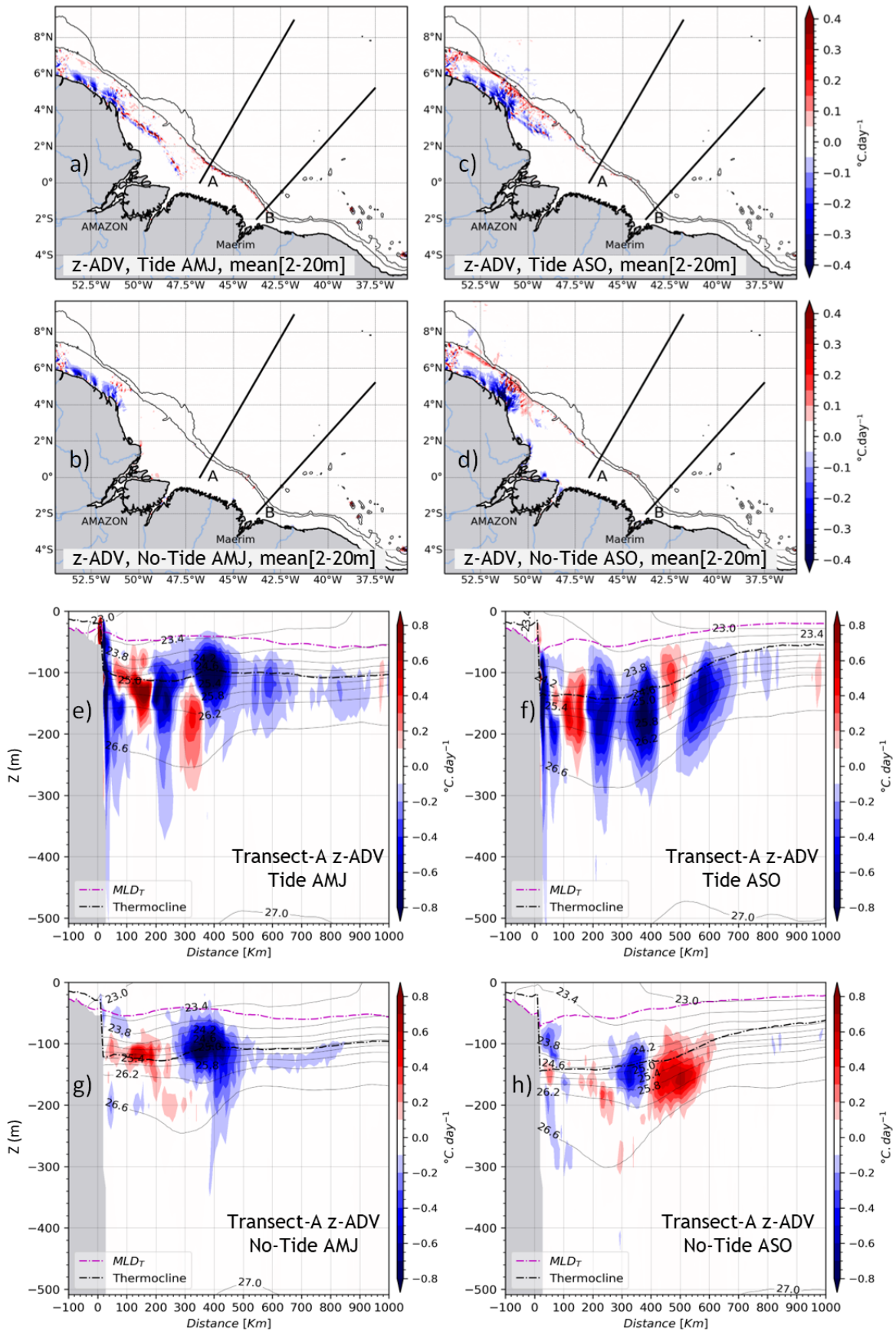
1371



1374 Figure 8. The vertical diffusion tendency of temperature (ZDF) for both seasons. The vertical
1375 mean between 2–20 m for AMJ season in tidal (a) and non-tidal (b) ~~simulations~~simulations;
1376 then for ASO season in tidal (c) and non-tidal (d) simulations. Vertical sections of ZDF
1377 following the transect A ~~for AMJ season in the tidal (e), for ASO season in non tidal (f)~~
1378 ~~simulations for (e) AMJ and (f) ASO seasons;~~ then for ~~AMJ season in the non-tidal~~ simulations
1379 for (g) AMJ and for(h) ASO season in the non-tidal (h) simulations. ~~The black and magenta~~
1380 ~~dashed lines are the thermocline depth and MLD respectively.~~ seasons. Solid black lines in
1381 panels a–d stand for the 200 m and 2000 m isobaths from the model bathymetry, while ~~in~~
1382 ~~panels e–h,~~ they represent the density (σ_θ) contours in panels e–h. ~~The magenta and black~~
1383 ~~dashed lines in panels e–h represent MLD and the thermocline depth, respectively.~~

1384
1385
1386
1387
1388
1389
1390
1391
1392
1393
1394
1395
1396
1397
1398
1399
1400
1401
1402
1403
1404
1405
1406
1407
1408
1409

1410
|
1411
|
1412



1414 *Figure 9. Same as figure 8, but for the vertical advection tendency of temperature (z-ADV).*

1415

1416

1417

1418

1419

1420

1421

1422

1423

1424

1425

1426

1427

1428

1429

1430

1431

1432

1433

1434

1435

1436

1437

1438

1439

1440

1441

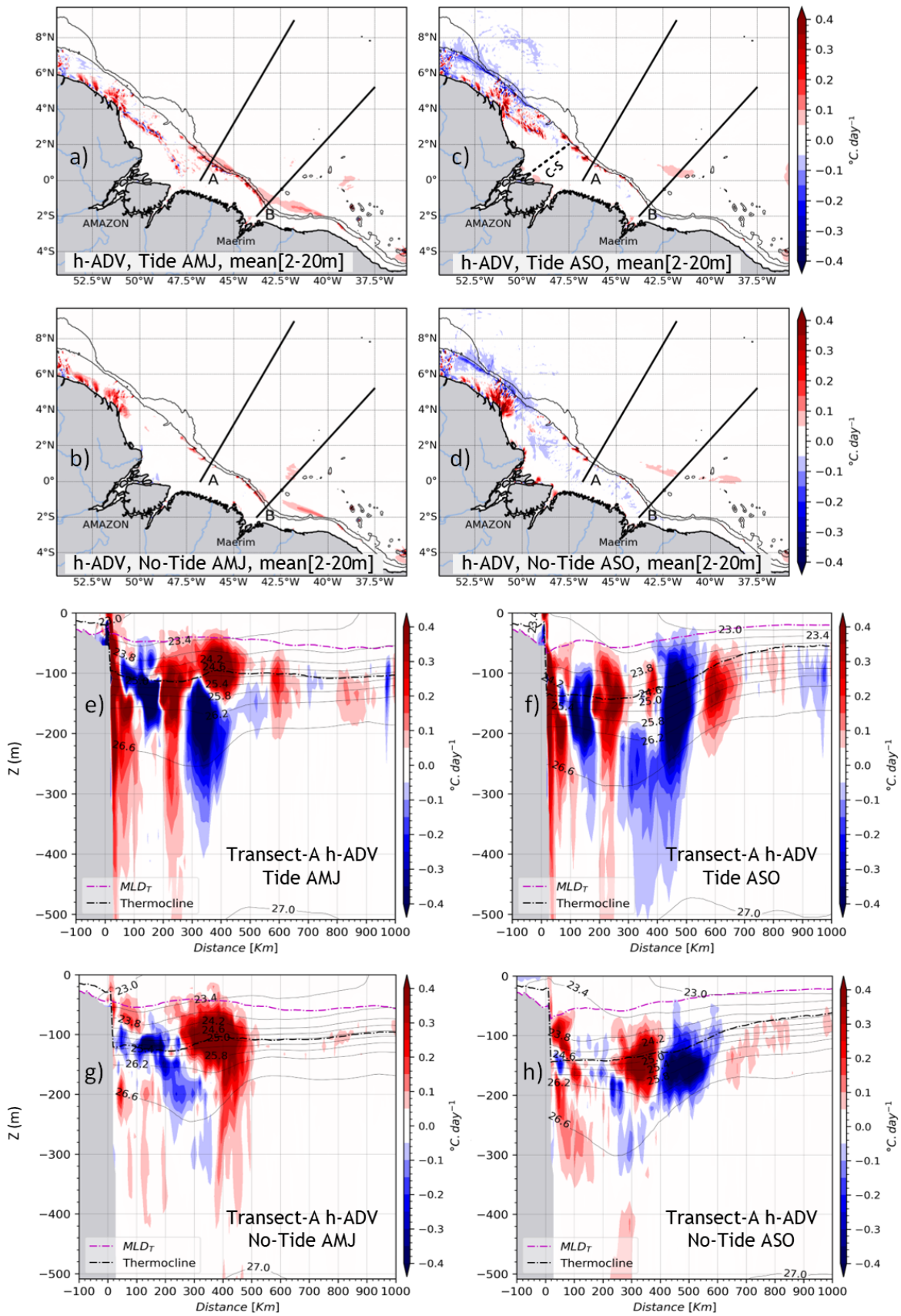
1442

1443

1444

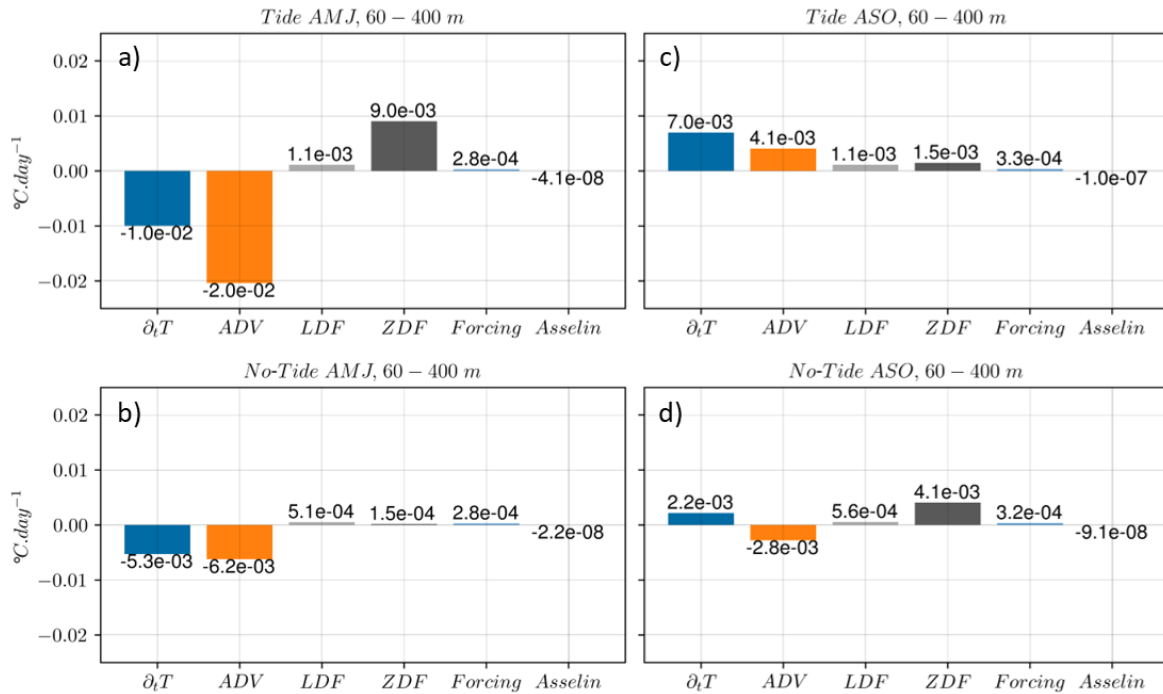
1445

1446

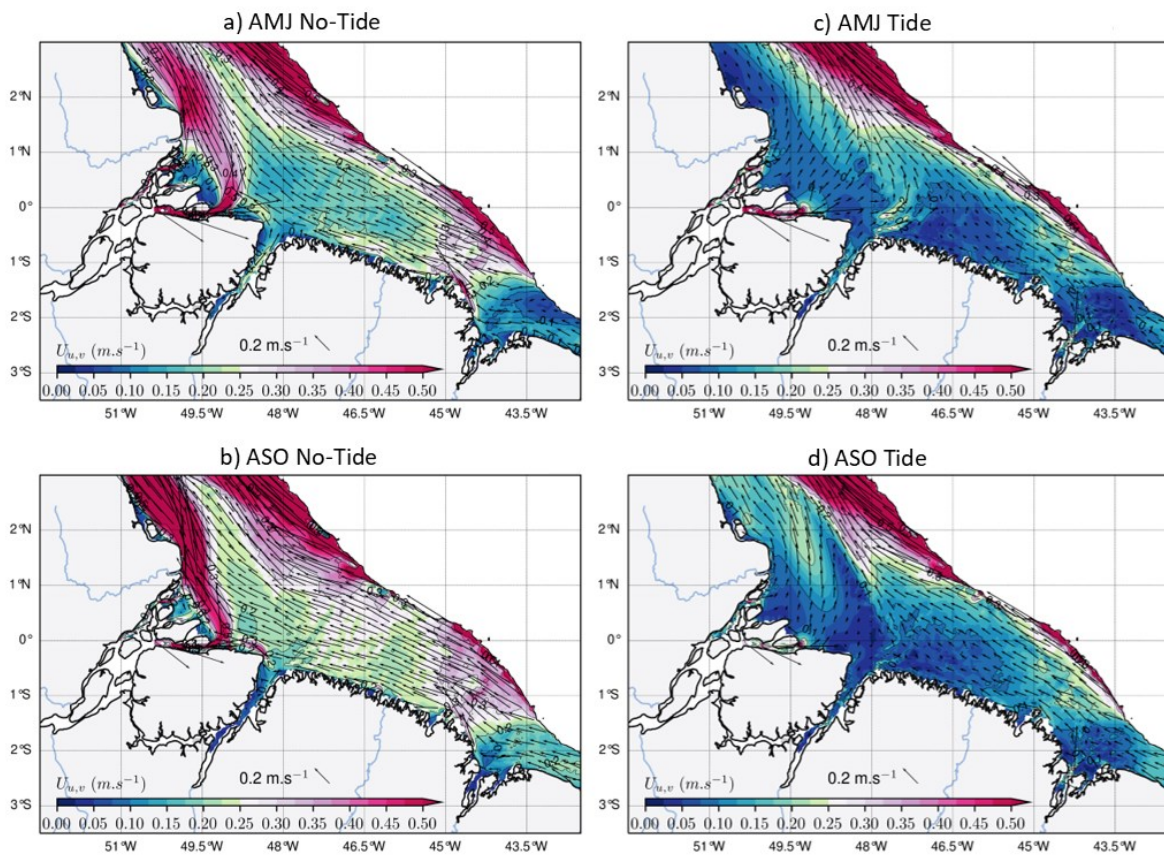


1448 Figure 10. Same as figure 8 but for the horizontal advection of temperature ($h_{-}ADV = x-ADV$
 1449 $+ y-ADV$). The dashed line from the Amazon River mouth toward the outer shelf in the panel
 1450 (b) indicates the cross-shore transect (C-S) used further on.
 1451

1452
 1453
 1454
 1455



1456 Figure 11. Trends balance Three-dimensional heat budget equation terms averaged in region
 1457 around IT trajectories between 48°W–40°W and 0°N–6°N, and below the MLD between 60–
 1458 400 m depth. Upper panels are for the tidal simulations and lower panels for the non-tidal
 1459 simulations, while left and right panels are for the AMJ and ASO seasons, respectively. ZDF is the dominant term of the heat budget equation (see section II.3.2) within
 1460 the mixed layer to explain temperature changes in upper layers.
 1461
 1462
 1463
 1464
 1465
 1466
 1467
 1468
 1469
 1470
 1471



1473

1474 *Figure 12. ~~The seasonal~~ Seasonal mean of the ~~mean~~ current ($U_{u,v}$) at the shelf averaged between*
 1475 *the surface and 50 m: the non-tidal ~~simulation~~ simulations in the left panels and the tidal*
 1476 *~~simulation~~ simulations in the right panels. The upper panels stand for ~~the~~ AMJ season, while*
 1477 *the lower stand for ~~the~~ ASO season. The color shading is the modulus of the current and the*
 1478 *black arrows represent its direction. Values beyond the 200 m isobath are masked.*

1479

1480

1481

1482

1483

1484

1485

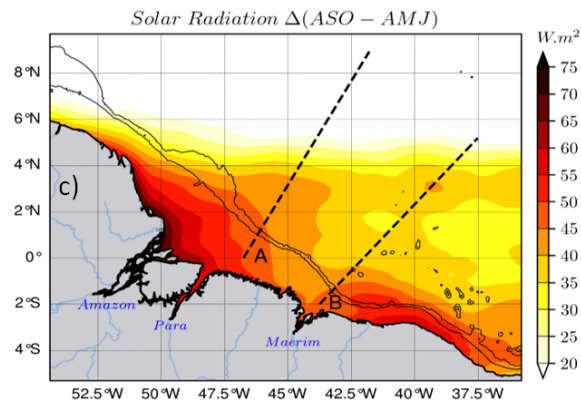
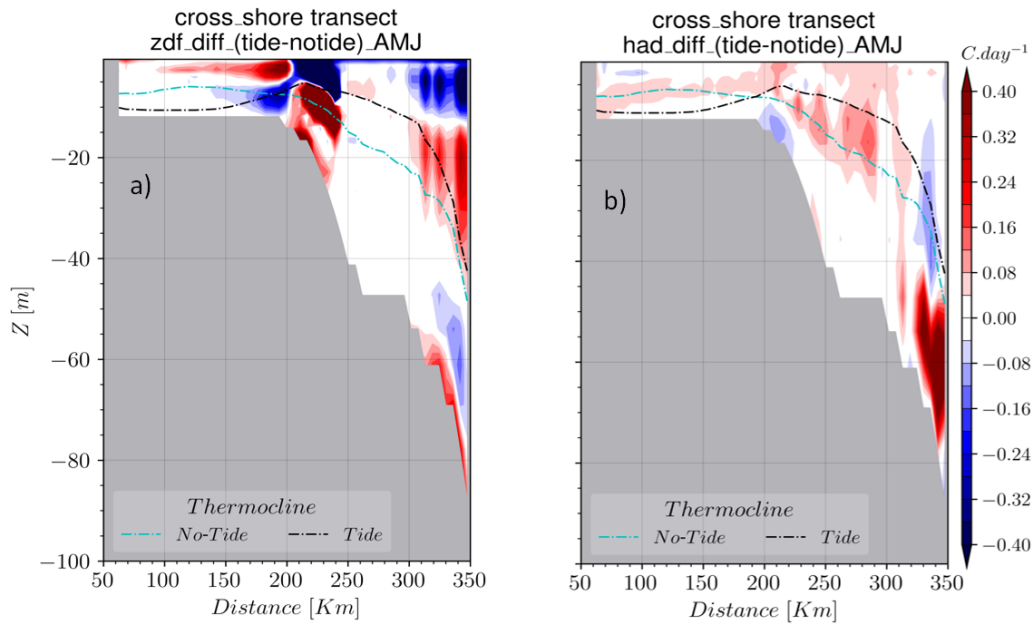
1486

1487

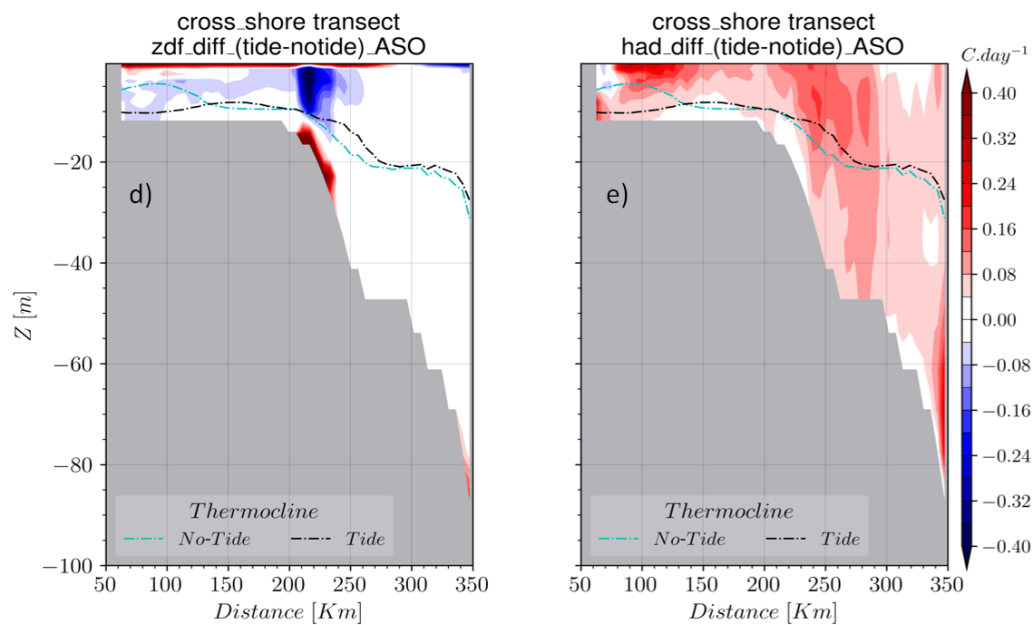
1488

1489

1490

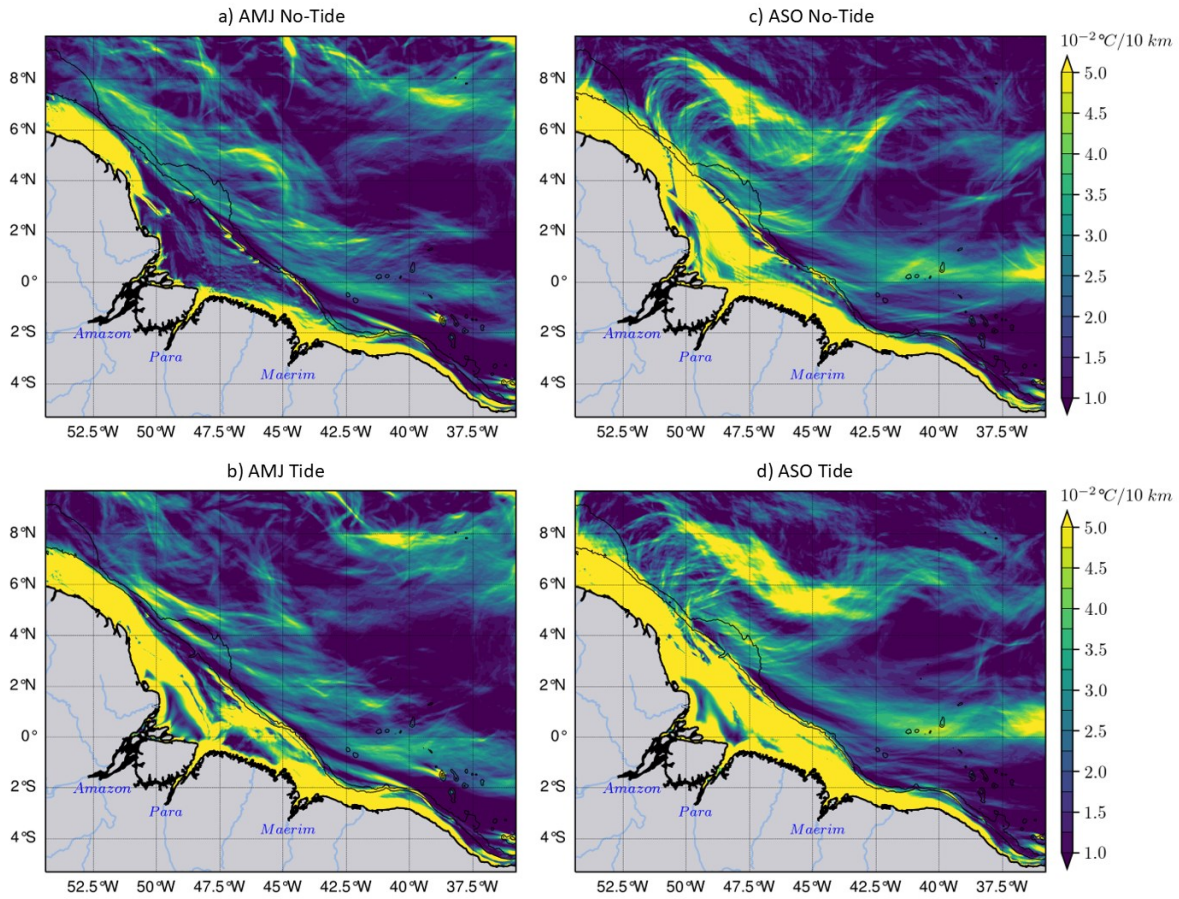


Solar radiation (Q_s) increases in the ASO season:
 > 30 $W \cdot m^2$ offshore
 > 60 $W \cdot m^2$ over the shelf



1493
 1494
 1495
 1496
 1497
 1498
 1499
 1500

Figure 13. The cross-shore transect of ZDF anomaly for (a) AMJ and (b) ASO seasons, ~~then~~ for h-ADV anomaly for (d) AMJ and (e) ASO seasons ; (e) Difference(c) difference in solar radiation between ASO and AMJ seasons. Solar radiation increases during the ASO season, with greater intensity on the shelf. The cross-shore transect of h-ADV anomaly for (d) AMJ and (e) ASO seasons.



1501
 1502
 1503
 1504
 1505
 1506
 1507
 1508
 1509
 1510
 1511
 1512
 1513

Figure 14. The horizontal gradient of the Temperature (∇T) averaged between 2–20 m-: the AMJ season in the left panels and ASO season in the right panels, the simulations without ~~the~~ tides in the upper panels, and with tides in the lower panels. During the ASO season, ~~the~~ stronger NBC retroflects in the north-west and eddy activity intensifies ~~in the north-west.~~ Therefore, ∇T emphasizes eddy-like fronts at the same location as eddy-like patterns in ~~ZDF~~ (see Fig. 9b).8c).